Anomalous proximity effects at the interface of s- and $s_\pm$- superconductors

Valentin G. Stanev and Alexei E. Koshelev
Materials Science Division, Argonne National Laboratory, Argonne, Illinois 60439, USA
(Received 13 August 2012; revised manuscript received 18 October 2012; published 19 November 2012)

We study proximity effects close to a boundary between s and $s_\pm$ superconductors. Frustration, caused by interaction of the s-wave gap parameter with the opposite-sign gaps of $s_\pm$ superconductor, leads to several anomalous features. In the case of strong frustration a nontrivial time-reversal-symmetry breaking (TRSB) state, with nonzero phase angles between all gap parameters, is possible. In a more typical state, the s-wave order parameter is aligned with one of the $s_\pm$ gaps. The other (antialigned) gap induces negative feature in the s-wave density of states, which can serve as a fingerprint of the $s_\pm$ state. Another consequence of the frustration is an extended region in the parameter space in which s-wave superconductivity is suppressed, despite being in contact with nominally stronger superconductor. This negative proximity effect is always present for the TRSB state, but extends even into the aligned states. We study these effects within a simple microscopic model assuming a dirty limit in all bands, which allows us to model the system in terms of minimum number of the most relevant parameters. The described anomalous features provide a route to establishing the possible $s_\pm$ state in the iron-based superconductors.

DOI: 10.1103/PhysRevB.86.174515 PACS number(s): 74.70.Xa, 74.20.Rp, 74.45.+c

I. INTRODUCTION

The discovery[1] of the iron-based high-temperature superconductors has brought new theoretical and experimental challenges to condensed matter physics. Despite the undoubted progress in our knowledge (see, for example, Refs. 2–4) some of the most intriguing questions still do not have a definite answer. First among them by importance is the precise form of the superconducting order parameter. The most plausible candidate so far is the extended s-wave or $s_\pm$ state.[5] In this state the gaps on the (holelike) bands at the center and the (electronlike) bands at corners of the Brillouin zone (BZ) have opposite signs. The physical origin of this state is in the repulsive interband interactions, which likely dominate the pairing in these materials. Although unconventional, such a state from symmetry point of view is indistinguishable from a conventional s-wave state, as they both belong to the A_{1g} representation of the lattice rotation group. Existence of such a state is supported by theoretical calculations done within the framework of several methods: random phase approximation (RPA),[6,7] functional renormalization group (FRG),[8,9] fluctuation exchange (FLEX),[10] as well as analytic one-loop RG and diagrammatic calculations.[11–14]

In spite of a concentrated effort, the structure of the order parameter in these superconductors has not yet been unambiguously established from experiment. The angle-resolved photoemission spectroscopy (ARPES) reveals uniform gaps on different bands[15] for several compounds close to optimal doping, but it cannot resolve the most crucial issue: the relative sign of the gaps in the electron and hole bands. This sign can be probed by some phase-sensitive experiments, similar to ones performed for the cuprate high-temperature superconductors.[16] Even though suggestions for such experiment have been made,[17,18] they have not been realized in practice yet.[19]

The strongest support in favor of the $s_\pm$ state comes from inelastic neutron scattering experiments,[20] which detect the emergence of a resonant magnetic mode below the superconducting transition, as expected for such a sign-changing state. This mode was detected in almost all iron-based superconductors and its frequency scales approximately proportional to transition temperature.[3] However, straightforward interpretation of the data is complicated by the multiband character of the Fermi surface (FS) and the possible strong role of interactions.

Another strong argument in favor of the $s_\pm$ state is microscopic coexistence of antiferromagnetism and superconductivity experimentally demonstrated in some compounds within a narrow doping range, most clearly in $Ba[Fe_{1-x}Co_x]_2As_2$ (Refs. 21 and 22). Spin-density wave (SDW) has strong pair-breaking effect on the conventional s_{++} state in which the order parameter has the same sign in all bands. Such direct pair breaking is absent if the order parameter has opposite signs in the bands connected by the SDW ordering wave vector, as was confirmed by several theoretical studies.[23] Thus, the SDW is much more compatible with the $s_\pm$ state than with s_{++} one.

Indirect probe of the bulk order parameter structure is provided by the low-temperature behavior of the thermodynamic and transport properties which is sensitive to the presence of quasiparticle states at the Fermi level. Extensive studies have demonstrated a very rich behavior; all compounds fall into three relatively well-defined groups. Several clean materials [LiFeAs (Ref. 24) and $Ba_{1-x}K_xFe_2As_2$ (Ref. 25)] do not show low-energy quasiparticles (they exhibit exponential temperature dependence of the London penetration depth and no residual linear term in the specific heat), meaning that all bands are fully gapped. Other materials, with weak impurity scattering, like LaFePO (Ref. 26), KFe_2As_2 (Ref. 27), and $BaFe_2[As_{1-x}P_x]_2$ (Ref. 28) shows behavior characteristic of a clean superconductor with line nodes of the gap parameter, namely, linear temperature dependence of the London penetration depth and square root magnetic field dependence of the thermal conductivity. Moreover, for $BaFe_2[As_{1-x}P_x]_2$ the presence of the node lines in one of the bands has been directly confirmed by ARPES.[29] Note that the existence of accidental nodes does not necessarily contradict the overall picture of the $s_\pm$ state; even though the order parameter may change sign

within one band, what matters most is the sign of its average value over the FS of this band. The third group of materials is formed by the compounds with strong scattering by dopants, such as $Ba[Fe_{1-x}Co_x]_2As_2$, which have rather large residual specific heat at low temperatures[30] and quadratic dependence of the London penetration depth[31] and typically show residual thermal conductivity.[32] These properties are not consistent with fully gapped s-wave order parameter. While this behavior can be interpreted as an indication for the accidental nodes of the gap in combination with strong impurity scattering, it is also compatible with $s_\pm$ state, where interband impurity scattering generates large number of subgap states and leads to finite density of states at the Fermi level.[33]

The discovery of another iron-based superconducting family[34]—the chalcogenide 122's—cast some doubts on the $s_\pm$ state as a universal state for all compounds, since in these materials the hole bands around the Γ point are absent. Possible pairing mechanisms and structures of the order parameter in view of recent experimental developments have been extensively discussed in recent reviews.[4]

In this paper we explore an alternative approach for probing the superconducting order parameter in iron-based materials. It is based on proximity effect, the mutual influence of two superconductors, brought in contact. We study the vicinity of a boundary between ordinary s-wave and $s_\pm$ superconductors (see Fig. 1). Competing interactions between the s-wave order parameter and $s_\pm$ gaps with opposite signs lead to frustration. As a consequence of this frustration, several interesting effects can appear, including the possibility of new superconducting

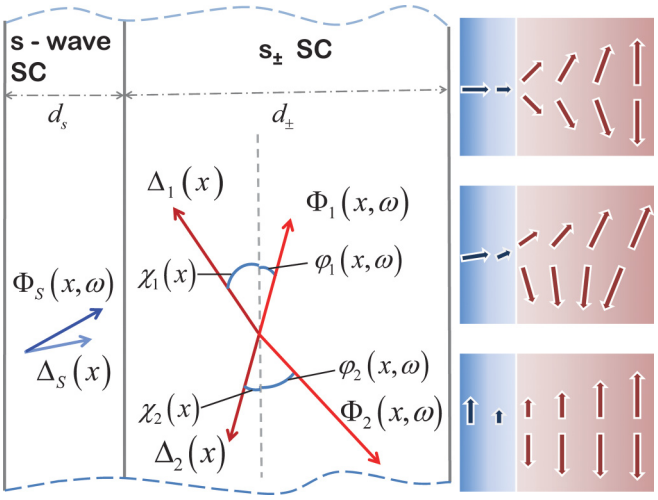

FIG. 1. (Color online) (Left) The proximity structure composed of s-wave and $s_\pm$ superconductors which we consider in this paper. The superconductors are described by the Green's functions Φ depending on coordinate x and Matsubara frequency ω and corresponding gap parameters $\Delta(x)$. For $s_\pm$ superconductor these parameters depend on the band index $\alpha = 1,2$ (see Sec. III for details). Φ_s couples to the Φ_α on the $s_\pm$ side. In the case of close coupling strengths with different bands, this creates the possibility for a nontrivial relative phases ϕ_α (as functions of x and ω) and the TRSB state. (Right) The three possible states. From top to bottom, we show the behavior of the anomalous part of the Greens' functions in the symmetric and asymmetric TRSB state and the aligned state.

states. This is in contrast with proximity between conventional (whether single- or multiband) superconductors, which is a rather straightforward phenomenon; the phases of the gaps on both sides always align and their amplitudes get closer (i.e., the smaller is enhanced and the larger is suppressed; see, for example, Ref. 35). In the case of a contact between s and $s_\pm$ superconductors there is no obvious way to align the phases and several possibilities compete.

Various effects close to a boundary between s and $s_\pm$ superconductors have been already considered. Both phenomenological and microscopic methods were used, a number of interesting and novel results were obtained, and different effects have been suggested as possible fingerprints of the $s_\pm$ state. Several papers have concentrated on the problem of a Josephson junction between s and $s_\pm$ superconductors[17,18,36,37] in the context of superconducting quantum interference device[17] and Josephson[18,36] interferometry and macroscopic quantum tunneling[37,38] (for a detailed review of the theoretical and experimental results see Ref. 39). In Refs. 40–43 the mutual effects of s and $s_\pm$ superconductors in contact were considered, and the possibility for a new time-reversal symmetry-breaking (TRSB) state close to the interface was discussed. The methods used to obtain the TRSB state were different; however, all of them have some intrinsic limitations and the obtained solutions cannot be regarded as fully microscopic and self-consistent.

In this paper we consider in detail anomalous features of a system composed of a two-band $s_\pm$ superconductor in contact with a weaker (i.e., with smaller bulk critical temperature) single-band s-wave superconductor (see Fig. 1). We employ simple microscopic model, which assumes a dirty limit in all superconductors but neglects interband scattering in $s_\pm$ superconductors. This model allows us to describe the system using a minimum number of the most essential and physically transparent parameters. Our approach neglects many features of iron pnictides, such as the presence of more than two gaps, interband scattering, orbital content of the bands, accidental nodes, etc., which may be relevant for detailed comparison of the theory with the experimental data. We believe, however, that the overall picture we present will survive even in a more realistic calculation.

As we show below, several nontrivial effects can be expected is such structures. If the s-wave superconductor is much stronger coupled to one of the gaps on the $s_\pm$ side than the other, it is natural to expect that its order parameter aligns with this gap. The phase of the gap in the other band is then antialigned with the s-wave gap and thus frustrated. This frustration leads to the possibility of negative proximity effect, the magnitudes of *all* gaps being suppressed close to the boundary (see the lower right panel on Fig. 1). This effect is unique to the interface with $s_\pm$ order parameter and has to be contrasted with the case of s-s_{++}-wave structures, where the smallest gap is always enhanced (we call this conventional proximity effect positive). As we demonstrate below, in the aligned state both positive and negative effects are possible. We again emphasize that the negative proximity effect cannot be present for conventional s-wave order parameter (assuming that the interface does not induce extrinsic pair-breaking). Thus, observation of such an effect will be a definitive proof of the presence of $s_\pm$ state in iron pnictides. The reverse is

not true; positive proximity effect is possible for both $s_\pm$- and s_{++}-wave superconductors.

When the properties of the two bands on the $s_\pm$ side are roughly the same, and the coupling across the boundary is identical, an even more interesting possibility arises.[40,41] Since the frustration in such a system is large, another state emerges as a compromise. In it the relative phase of the gaps on the $s_\pm$ side deviates from its bulk π value close to the boundary. This tilting relieves some of the frustration due to the interboundary coupling and disappears in the bulk (see the top right panel in Fig. 1). Such a state is intrinsically complex and thus breaks the time-reversal symmetry.[44] Due to the finite phase difference between the gaps, it is characterized by spontaneous supercurrents with opposite direction flowing between the s-superconductor and $s_\pm$ bands so that in the ground state the total supercurrent is zero. In a more general situation of different $s_\pm$ gaps, the TRSB state is possible when the Josephson coupling energies between the s-wave order parameter and the opposite-sign bands exactly compensate each other. Another interesting consequence of our results is the possible phase transitions between these different superconducting states. The direct way to induce the TRSB state is to vary the asymmetry. Unfortunately, there is no obvious way to do this. More relevant experimentally are the transitions tuned by the temperature. Within some range of parameters the aligned state is stable at higher temperature, but is supplanted by the TRSB state at lower temperatures through a phase transition.[45]

We focus on the situation when the direct interband reflection at the interface is negligible, which is expected, for example, for the contact made at the [001] surface of iron-based superconductor. In the opposite situation, when the interband reflection is strong, a different kind of the TRSB state has been predicted recently.[46]

In addition to these general effects we also consider the behavior of the density of states (DoS) on both sides of the s-$s_\pm$ interface. This quantity can be directly measured using the tunneling conductivity. As we show, in the aligned state the aligned/antialigned gap induces positive/negative correction in the s-wave DoS. Thus, observation of these features can be used to probe the multiband order parameter (see also Ref. 47).

It is instructive to compare properties of the $s/s_\pm$ proximity system considered in this paper with interfaces between s- and d-wave superconductors, because d-wave represents a prominent case of sign-changing order parameter realized in cuprate superconductors. The properties of the such interfaces have been studied quite extensively (see, e.g., Refs. 48–50), and several similar anomalous features have been reported. In particular, for certain orientations the free surface of d-wave superconductors or s/d interface may generate $d+is$ or $d_{x^2-y^2}+id_{xy}$ states with broken time-reversal symmetry.[50,51] In contrast to the situation we consider here, these states are induced by quasiparticle reflection at the interface between the different-sign lobes. It was also found that the sign of proximity effect may be negative for both superconductors,[49] but the conditions for this phenomenon were not studied in detail. The proximity corrections induced by the d-wave superconductor into the s-wave DoS have been studied in Refs. 49 and 50. The most prominent feature is the peak near zero energy due to the Andreev bound state which splits when the TRSB state is formed at the interface. Also, a smooth peak is typically formed at the energy corresponding to the maximum gap of d-wave superconductor.

Let us outline the structure of the paper. First, in Sec. II we present a very simple phenomenological model of a frustrated Josephson junction. In spite of its simplicity, we believe that this model catches some of the essential physics of the system. The results we obtain agree with the intuitive picture we presented above: The TRSB state is stable when the Josephson couplings with the opposite-sign bands are very close, corresponding to strong frustration. Away from this region, the aligned states are more favorable. The frustrated Josephson junction model predicts continuous phase transitions between the aligned and TRSB states.

The above simple model, however, does not describe proximity effects and misses other important details as well. To develop a more realistic description of the superconductivity on both sides of the interface, we use microscopic theory in the dirty limit presented in Sec. III, which describes the system by multiband Usadel equations supplemented with the appropriate boundary conditions. In Sec. IV we present analytical results obtained in the limit of weak coupling between the superconductors, and in Sec. V we describe the procedure used for numerical solution of the equations. Even though this approach is strictly applicable only in the dirty limit, we expect our results to be qualitatively (or even quantitatively) correct in the clean case as well.

Within the developed framework we study different superconducting states. We start with the more conventional aligned state (in Sec. VI) and obtain both positive and negative proximity effects, depending on the values of different physical parameters. In Sec. VII we show that the TRSB state indeed exists and develop its quantitative description. Furthermore, the proximity effect for such a state is always negative (this is also clear from general considerations). In Sec. VIII we summarize our results and discuss the possible limitations of our approach.

II. SIMPLE MODEL: FRUSTRATED JOSEPHSON JUNCTION

To gain some insight into the phase diagram of the system let us first consider a simple phenomenological model, which nevertheless catches essential physics: Josephson junction between s and $s_\pm$ superconductors (see also Ref. 43). The energy of such systems depends on the phase shifts between the order parameters in the bands of the $s_\pm$ superconductor and the order parameter in the s-wave superconductor, $\theta_{1,2}=\phi_{1,2}-\phi_s$. On general grounds, the simplest form of this energy in reduced form can be written as

$$E(\theta_1,\theta_2)=\cos(\theta_1-\theta_2)-t_1\cos\theta_1-t_2\cos\theta_2, \qquad (1)$$

with

$$t_\alpha=E_{J,\alpha}/\mathcal{E}_{12}d_\pm\ll 1,$$

where $E_{J,\alpha}$ are Josephson coupling energies between the s-wave superconductor and two bands of the $s_\pm$ superconductors, $\mathcal{E}_{12}$ is the interband coupling energy, and $d_\pm$ is the thickness of the $s_\pm$ superconductor. For definiteness, we assume $t_1\geqslant t_2$.

Minimizing the energy, we get the equilibrium conditions

$$-\sin(\theta_1-\theta_2)+t_1\sin\theta_1=0, \tag{2a}$$

$$\sin(\theta_1-\theta_2)+t_2\sin\theta_2=0, \tag{2b}$$

and, as a consequence,

$$t_1\sin\theta_1=-t_2\sin\theta_2. \tag{2c}$$

Excluding θ_2, we obtain an equation for θ_1,

$$\sin\theta_1\left(-\sqrt{1-\frac{t_1^2}{t_2^2}\sin^2\theta_1}-\cos\theta_1\frac{t_1}{t_2}+t_1\right)=0.$$

This equation has two solutions, corresponding to the aligned and TRSB states. For the aligned state, $\sin\theta_1=0$ and we obtain $\theta_1=0$, $\theta_2=\pi$, and

$$E_{\rm al}=-1-t_1+t_2. \tag{3}$$

For the TRSB state we obtain

$$\cos\theta_1=\frac{t_2}{2}+\frac{1}{2t_2}-\frac{t_2}{2t_1^2}, \tag{4a}$$

$$\cos\theta_2=\frac{t_1}{2}+\frac{1}{2t_1}-\frac{t_1}{2t_2^2}. \tag{4b}$$

In particular, for the symmetric case $t_1=t_2$, and we have $\cos\theta_1=\cos\theta_2=t_1/2$. The energy for the frustrated state can be written as

$$E_{\rm fr}=-\tfrac{1}{2}\left(t_1t_2+t_2/t_1+t_1/t_2\right). \tag{5}$$

The transition to the aligned state occurs when $\cos\theta_1=1$, giving

$$t_2=\frac{t_1}{1+t_1}, \tag{6}$$

and the aligned state is stable for $t_2<t_1/(1+t_1)$. Converting to real units, we conclude that, for weak Josephson coupling, the frustrated state is realized in the region $|E_{J,1}-E_{J,2}|<E_J^2/(\mathcal{E}_{12}d_\pm)$.

These results are summarized on Fig. 2. As we have anticipated, the TRSB state exists in the region where the frustration is maximum ($t_1\approx t_2$), and is replaced by the aligned state when one of the couplings dominates. The transition between the two states is continuous. Even though this simple model cannot pretend to give quantitative description of the interface, we expect that its general features survive in a more microscopic setup, which we now proceed to describe.

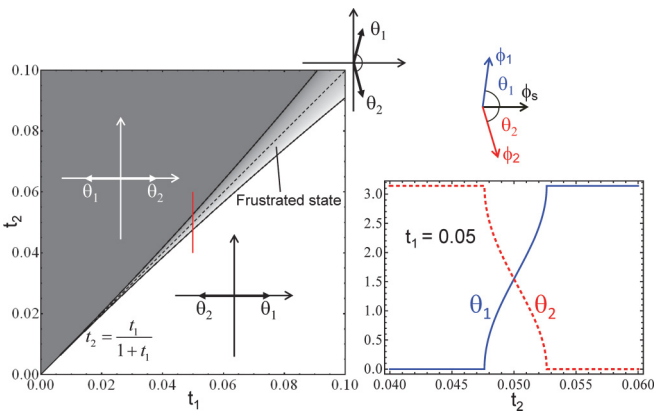

FIG. 2. (Color online) (Left) The phase diagram of a frustrated Josephson junction. The TRSB state exists near the diagonal part where $t_1\approx t_2$. Away from this diagonal region the aligned state is realized. (Right) Evolution of the phase angles $\theta_{1,2}$ along the vertical line marked in the phase diagram.

III. USADEL EQUATIONS AND BOUNDARY CONDITIONS

We now move to a microscopic description of the problem. Let us consider a "sandwich," consisting of a slab of a two-band $s_\pm$ superconductor with thickness $d_\pm$, in contact with a slab of a single-band s-wave superconductor with thickness d_s, as shown in Fig. 1. We choose the $x=0$ plane to be the boundary between the two layers. The main assumption of our description is that both superconductors are in the dirty limit, but the *interband* scattering in the $s_\pm$ superconductor is negligible. In this case superconductivity can be described by a simplified version of the Gor'kov equations, known as Usadel equations.[52] The following formalism has been developed in Ref. 53 and applied to the case of conventional two-band superconductors in Ref. 35.

For the s-wave superconductor ($-d_s<x<0$), the equations for the impurity averaged Greens' functions G_s and Φ_s (where $\Phi_s=\omega F_s/G_s$ and F_s is the anomalous part of the single-particle Green's function), with the necessary self-consistency equation, are

$$\frac{D_s}{2\omega G_s}\left[G_s^2\Phi_s'\right]'-\Phi_s=-\Delta_s, \tag{7a}$$

$$2\pi T\sum_{\omega>0}\lambda_s\frac{G_s\Phi_s}{\omega}=\Delta_s,\quad G_s=\frac{\omega}{\sqrt{\omega^2+|\Phi_s|^2}}, \tag{7b}$$

where the prime denotes spatial derivative, and $\omega=2\pi T(n+1/2)$ stands for the Matsubara frequencies.

For the $s_\pm$ superconductor, $0<x<d_\pm$, and the band index $\alpha=1,2$, we have

$$\frac{D_\alpha}{2\omega G_\alpha}\left[G_\alpha^2\Phi_\alpha'\right]'-\Phi_\alpha=-\Delta_\alpha, \tag{8a}$$

$$2\pi T\sum_{\beta,\ \omega>0}\lambda_{\alpha\beta}\frac{G_\beta\Phi_\beta}{\omega}=\Delta_\alpha,\quad G_\alpha=\frac{\omega}{\sqrt{\omega^2+|\Phi_\alpha|^2}} \tag{8b}$$

(we again emphasize the fact that interband impurity scattering has been neglected; for details see Ref. 35 and Sec. VIII). We denote the bulk critical temperatures of the $s_\pm$ and s-wave superconductors as T_c and T_c^s, respectively. Since we consider $s_\pm$ superconductor, we assume $\Delta_1\Delta_2<0$ which is realized if $\lambda_{12},\lambda_{21}<0$. The diffusion coefficients $D_{\{s,\alpha\}}$ are related to the conductivities $\sigma_{\{s,\alpha\}}$ as $\sigma_{\{s,\alpha\}}=e^2\nu_{\{s,\alpha\}}D_{\{s,\alpha\}}$, where $\nu_{\{s,\alpha\}}$ are the normal DoSs. The ratio of the off-diagonal coupling constants is given by the ratio of partial normal DoSs, $\lambda_{\alpha\beta}/\lambda_{\beta\alpha}=\nu_\beta/\nu_\alpha$. It is convenient to normalize all energy scales (ω and gaps on *both* sides) to πT_c. We also introduce coherence lengths $\xi_\alpha=\sqrt{D_\alpha/2\pi T_c}$ and $\xi_s^*=\sqrt{D_s/2\pi T_c}$ (note that ξ_s^* is related to the true bulk coherence length of the s-wave superconductor by $\xi_s=\xi_s^*\sqrt{T_c/T_c^s}$).

Since we consider an interface, these equations have to be supplemented with appropriate boundary conditions. These connect the Green's functions and their derivatives at the $x=0$

plane and can be written as[54]

$$\xi_s^* G_s^2 \Phi_s' = \sum_\alpha \frac{\xi_\alpha}{\gamma_\alpha} G_\alpha^2 \Phi_\alpha', \tag{9a}$$

$$\xi_\alpha G_\alpha \Phi_\alpha' = -\frac{1}{\gamma_{B\alpha}} G_s(\Phi_s - \Phi_\alpha), \tag{9b}$$

for $\alpha = 1,2$ with

$$\gamma_\alpha = \frac{\rho_\alpha \xi_\alpha}{\rho_s \xi_s^*}, \quad \gamma_{B\alpha} = \frac{R_{B\alpha}}{\xi_\alpha \rho_\alpha}, \tag{10}$$

where ρ_s and ρ_α are the bulk resistivities of the s-wave superconductor and the α band and $R_{B\alpha}$ is the boundary resistivity for band α. We can combine Eqs. (9a) and (9b) and get the useful equivalent form of the boundary condition (9a),

$$\xi_s^* G_s \Phi_s' = \sum_\alpha \frac{1}{\tilde{\gamma}_{B\alpha}} G_\alpha(\Phi_\alpha - \Phi_s), \tag{11}$$

where we introduced the new interface parameters $\tilde{\gamma}_{B\alpha} = \gamma_{B\alpha}\gamma_\alpha$, which we use together with $\gamma_{B\alpha}$. We also have to specify the conditions on the external boundaries:

$$\Phi_s'(-d_s) = 0, \;\; \Phi_\alpha'(d_\pm) = 0. \tag{12}$$

Four parameters enter the boundary conditions and control the strength and the sign of the proximity effect; γ_1 and γ_2 depend on the bulk properties of the materials, whereas γ_{B1} and γ_{B2} describe the boundary itself.[55] The first two parameters determine the relative strength of the proximity effect between the s-wave superconductor and the $s_\pm$ bands. In particular, large γ_α implies that the s-wave material is more metallic than the α band on the $s_\pm$ side, and thus strongly influences it through proximity, while remaining weakly affected by this band itself. For the ratio of these parameters we derive the following relation

$$\frac{\gamma_1}{\gamma_2} = \frac{\nu_2 \xi_2}{\nu_1 \xi_1} = \frac{\lambda_{12}\xi_2}{\lambda_{21}\xi_1}. \tag{13}$$

The parameter $\gamma_{B\alpha}$ is inversely proportional to the transparency of the boundary for the α band. Estimating these parameters is not easy, but for the case of iron-based materials (which are semimetals) in contact with typical conventional superconductor, we generally expect γ_α to be large.

To find the density of states, we have to perform analytical continuation of the Green's functions to real energies $i\omega \to E + i\delta$. The normalized DoS is related to the real-energy Green's function by the standard expression

$$N_{\{s,\alpha\}}(E,x) = \mathrm{Re}[G_{\{s,\alpha\}}(E,x)] = \mathrm{Re}\left[\frac{E}{\sqrt{E^2 - \Phi_{\{s,\alpha\}}(E,x)\Phi^*_{\{s,\alpha\}}(-E,x)}}\right]. \tag{14}$$

In the following section we present analytical results for the Green's functions and gap parameters obtained in the limit of weak coupling between superconductors (large $\gamma_{B\alpha}$) in the case of aligned state.

Establishing the model parameters which would describe real materials requires experimental determination of electronic and scattering properties of the individual bands. While this is a challenging task, in principle, this can be done using ARPES,[15,29] quantum oscillations,[56] or multiple-band fits of the magnetotransport[57] and optical measurements.[58]

IV. ANALYTICAL RESULTS FOR WEAK COUPLING

In the case of the weak coupling between s and $s_\pm$ superconductors, $\gamma_{B\alpha} \gg 1$, the contact-induced corrections to the gaps and Green's function can be treated as small perturbations, $\Delta_{\{s,\alpha\}}(x) = \Delta_{\{s,\alpha\}0} + \tilde{\Delta}_{\{s,\alpha\}}(x)$, $\Phi_{\{s,\alpha\}}(x) = \Delta_{\{s,\alpha\}0} + \tilde{\Phi}_{\{s,\alpha\}}(x)$. The small corrections $\tilde{\Phi}_{\{s,\alpha\}}(\omega,x)$ and $\tilde{\Delta}_{\{s,\alpha\}}(x)$ can be computed analytically in the linear order with respect to $1/\gamma_{B\alpha}$. Similar calculation for several types of junctions using somewhat different approach has been done in Ref. 59. We consider here only the case of aligned gaps. The computation details are presented in Appendix A and general results can be presented in the form of Fourier expansions. For the s-wave superconductor $\tilde{\Phi}_s(\omega,x) = \sum_{m=0}^\infty \tilde{\Phi}_{s,m}(\omega)\cos k_m x$ and $\tilde{\Delta}_s(x) = \sum_{m=0}^\infty \tilde{\Delta}_{s,m}\cos k_m x$ with $k_m = m\pi/d_s$ and the Fourier components are

$$\tilde{\Phi}_{s,m}(\omega) = \frac{\tilde{\Delta}_{s,m}}{1+\xi_{s,\omega}^2 k_m^2} - \frac{(2-\delta_m)\xi_{s,\omega}^2/(d_s\xi_s^*)}{1+\xi_{s,\omega}^2 k_m^2} \times \sum_\alpha \frac{\sqrt{\omega^2+\Delta_{s0}^2}}{\sqrt{\omega^2+\Delta_{\alpha0}^2}} \frac{\Delta_{s0}-\Delta_{\alpha0}}{\tilde{\gamma}_{B\alpha}}, \tag{15a}$$

$$\tilde{\Delta}_{s,m} = -\frac{2\pi T}{Z_{s,m}} \sum_{\alpha,\omega>0} \frac{\omega^2}{(\omega^2+\Delta_{s0}^2)\sqrt{\omega^2+\Delta_{\alpha0}^2}} \times \frac{(2-\delta_m)\xi_{s,\omega}^2/(d_s\xi_s^*)}{1+\xi_{s,\omega}^2 k_m^2} \frac{\Delta_{s0}-\Delta_{\alpha0}}{\tilde{\gamma}_{B\alpha}},$$

$$Z_{s,m} = 2\pi T \sum_{\omega>0} \frac{1}{(\omega^2+\Delta_{s0}^2)^{3/2}} \left(\Delta_{s0}^2 + \omega^2 \frac{\xi_{s,\omega}^2 k_m^2}{1+\xi_{s,\omega}^2 k_m^2}\right), \tag{15b}$$

where $\xi_{s,\omega}^2 = D_s/(2\sqrt{\omega^2+\Delta_{s0}^2})$.

For the $s_\pm$ superconductor the corresponding expansions are $\tilde{\Phi}_\alpha = \sum_{m=0}^\infty \tilde{\Phi}_{\alpha,m}\cos q_m x$, $\tilde{\Delta}_\alpha = \sum_{m=0}^\infty \tilde{\Delta}_{\alpha,m}\cos q_m x$ with $q_m = m\pi/d_\pm$. The Fourier components $\tilde{\Phi}_{\alpha,m}$ and $\tilde{\Delta}_{\alpha,m}$ are given by somewhat cumbersome but closed analytical formulas,

$$\tilde{\Phi}_{\alpha,m} = \frac{\tilde{\Delta}_{\alpha,m}}{1+\xi_{\alpha,\omega}^2 q_m^2} + \frac{(2-\delta_m)\xi_{\alpha,\omega}^2/(d_\pm\xi_\alpha)}{1+\xi_{\alpha,\omega}^2 q_m^2} \times \frac{\sqrt{\omega^2+\Delta_{\alpha0}^2}}{\sqrt{\omega^2+\Delta_{s0}^2}} \frac{\Delta_{s0}-\Delta_{\alpha0}}{\gamma_{B\alpha}}, \tag{16a}$$

$$\tilde{\Delta}_{\alpha,m} = 2\pi T \sum_{\beta,\omega>0} U_{m,\alpha\beta} \frac{\omega^2}{(\omega^2+\Delta_{\beta0}^2)\sqrt{\omega^2+\Delta_{s0}^2}} \times \frac{(2-\delta_m)\xi_{\beta,\omega}^2/(d_\pm\xi_\beta)}{1+\xi_{\beta,\omega}^2 q_m^2} \frac{\Delta_{s0}-\Delta_{\beta0}}{\gamma_{B\beta}}, \tag{16b}$$

and $\xi^2_{\alpha,\omega} \equiv D_\alpha/(2\sqrt{\omega^2+\Delta^2_{\alpha 0}})$. Here the matrix $U_{m,\alpha\beta}$ is defined by the relations

$$\hat{U}_m = \frac{1}{D_U}\begin{bmatrix} w_{22}-\Sigma_{m,2} & -w_{12} \\ -w_{21} & w_{11}-\Sigma_{m,1}\end{bmatrix},$$
$$D_U = -\Sigma_{m,2}w_{11}-\Sigma_{m,1}w_{22}+\Sigma_{m,1}\Sigma_{m,2},$$

with

$$\Sigma_{m,\alpha} = 2\pi T\sum_{\omega>0}\left[\frac{\omega^2}{\left(\omega^2+\Delta^2_{\alpha 0}\right)^{3/2}}\frac{1}{1+\xi^2_{\alpha,\omega}q_m^2}-\frac{1}{\omega}\right]+\ln\frac{1}{t}$$

and $\hat{w} = \hat{\lambda}^{-1} - \lambda^{-1}\hat{I}$ being the degenerate matrix whose components are given by relations

$$w_{11} = \frac{\sqrt{\lambda_-^2/4+\lambda_{12}\lambda_{21}}-\lambda_-/2}{\det\lambda}, \quad w_{12} = -\frac{\lambda_{12}}{\det\lambda},$$
$$w_{22} = \frac{\sqrt{\lambda_-^2/4+\lambda_{12}\lambda_{21}}+\lambda_-/2}{\det\lambda},$$

where $\lambda_- \equiv \lambda_{11}-\lambda_{22}$ and $\det\lambda \equiv \lambda_{11}\lambda_{22}-\lambda_{12}\lambda_{21}$.

The quantity $\tilde{\Delta}_{s,0}$ represents the average correction to the s-wave gap parameter induced by the contact. In particular, the sign of $\tilde{\Delta}_{s,0}$ determines wether s-wave superconductivity is enhanced or suppressed (positive vs negative proximity effect). At low temperatures it is possible to obtain an analytical result for the average gap correction (see Appendix A),

$$\frac{\tilde{\Delta}_{s,0}}{\pi T_c} = \frac{\xi_s^*}{d_s}\sum_\alpha U\left(\frac{\Delta_{s0}}{|\Delta_{\alpha 0}|}\right)\frac{\Delta_{\alpha 0}-\Delta_{s0}}{\tilde{\gamma}_{B\alpha}|\Delta_{\alpha 0}|},$$
$$\text{with} \quad U(a) = \frac{K(1-a^2)-E(1-a^2)}{1-a^2}, \tag{17}$$

where $K(m) = \int_0^{\pi/2}(1-m\sin^2\theta)^{-1/2}d\theta$ and $E(m) = \int_0^{\pi/2}(1-m\sin^2\theta)^{1/2}d\theta$ are the complete elliptic integrals. This general result further simplifies for the important particular case $\Delta_{s0} \ll |\Delta_{\alpha 0}|$. In this limit the elliptic integrals can be expressed in terms of elemental functions leading to

$$\frac{\tilde{\Delta}_{s,0}}{\pi T_c} \approx \frac{\xi_s^*}{d_s}\sum_\alpha \frac{\Delta_{\alpha 0}-\Delta_{s0}}{\tilde{\gamma}_{B\alpha}|\Delta_{\alpha 0}|}\left[\ln\left(\frac{4|\Delta_{\alpha 0}|}{\Delta_{s0}}\right)-1\right]. \tag{18}$$

From this result we can see that the partial contribution from the band is mostly determined by the strength of coupling to this band $\propto 1/\tilde{\gamma}_{B\alpha}$. In addition, we observe that while the positive contribution from the aligned band is proportional to the gap difference $\Delta_{10}-\Delta_{s0}$, the negative contribution from the antialigned band is proportional to the sum of the absolute gap values $|\Delta_{20}|+\Delta_{s0}$. As a consequence, even in the aligned state the negative contribution may exceed the positive one leading to the total negative proximity effect. This negative-proximity region is especially broad in the case when the gap values $\Delta_{\alpha 0}$ and Δ_{s0} are close. Figure 3 illustrates regions of positive and negative proximity in the coupling-constants plane, $1/\tilde{\gamma}_{B1}$-$1/\tilde{\gamma}_{B2}$, obtained using Eq. (17). The cases of identical and different $s_\pm$ gaps are illustrated. We can see that in both cases the region of negative proximity occupies a significant region in the parameter space.

To find corrections to the densities of states, $\delta N_s(E)$ and $\delta N_\alpha(E)$, we have to perform the analytical continuation

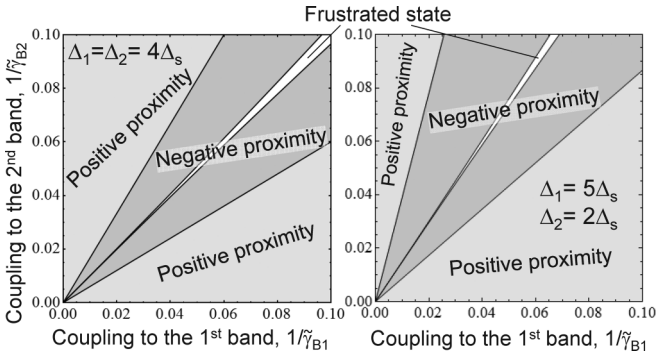

FIG. 3. The regions of positive and negative proximity in the weak-coupling regime evaluated using Eq. (17). The left and right diagrams illustrate, respectively, the cases of identical and different $s_\pm$ gaps.

$i\omega \to E+i\delta$ in Eqs. (15a) and (16a) and perform expansion in Eq. (14), which gives

$$\delta N_{\{s,\alpha\}0}(E,x) = \mathrm{Re}\left[\frac{E\Delta^*_{\{s,\alpha\}0}\tilde{\Phi}_{\{s,\alpha\}}(E,x)}{(E^2-|\Delta_{\{s,\alpha\}0}|^2)^{3/2}}\right]. \tag{19}$$

Simple analytical result illustrating general trends can be obtained at low temperatures in the case of thin s layer, $d_s < \xi_s$, and weak s-wave superconductor, $|\Delta_\alpha| \gg |\Delta_s|$.[47] In this case, the real-energy Green's function can be approximately evaluated as

$$\tilde{\Phi}_s(E,x) \approx \tilde{\Delta}_{s,0} - \pi T_c\frac{\xi_s^*}{d_s}\sum_\alpha\frac{1}{\sqrt{\Delta^2_{\alpha 0}-E^2}}\frac{\Delta_{s0}-\Delta_{\alpha 0}}{\tilde{\gamma}_{B\alpha}}. \tag{20}$$

Neglecting the first trivial term, we obtain the correction to the s-wave DoS

$$\delta N_s(E,x) \approx \pi T_c\frac{\xi_s^*}{d_s}\frac{E\Delta_{s0}}{\left(E^2-\Delta^2_{s0}\right)^{3/2}} \times\sum_\alpha\frac{\Delta_{\alpha 0}-\Delta_{s0}}{\tilde{\gamma}_{B\alpha}\sqrt{\Delta^2_{\alpha 0}-E^2}}\Theta\left(|\Delta_{\alpha 0}|-E\right), \tag{21}$$

where $\Theta(x)$ is the step function. We see that the aligned bands (positive Δ_α) induce positive corrections to the s-wave DoS and the antialigned bands (negative Δ_α) induce negative corrections. These negative features can serve as definite fingerprint of the $s_\pm$ state.[47] Note that the perturbative result (21) does not describes energy regions in the vicinity of the gap values, $E \sim |\Delta_{\alpha 0}|$.

To go beyond the weak-coupling regime we have to rely on numerical calculations. In the following section we describe numerical procedures and present results of these calculations for different cases.

V. NUMERICAL PROCEDURE

For numerical modeling, it is convenient to use the so-called θ parametrization, in which we write $G_s = \cos\theta_s$, $G_\alpha = \cos\theta_\alpha$. For Φ_α and Φ_s two choices will prove convenient. Let us first consider the (technically simpler) case of a significant difference between the coupling of one of the two gaps on the $s_\pm$ side to the gap on the s-wave side (weakly frustrated

interface). As already mentioned in the Introduction, in such situation we expect the so-called aligned state to be stable. In it the phase of Φ_s is aligned with one of Φ_α, while the phase difference between Φ_1 and Φ_2 is π; this state obviously belongs to the general class of $s_\pm$ states. Proximity effect on the s-wave side enters through the (asymmetric) suppression of Δ_1 and Δ_2 close to the boundary (schematically shown on the bottom right panel of Fig. 1).

In this state Φ_α and Φ_s can be chosen real, $\Phi_{\{s,\alpha\}} = \omega \tan\theta_{\{s,\alpha\}}$ (with the condition $\Phi_1\Phi_2 < 0$). In the following, we assume that the coherence lengths of the $s_\pm$ bands are equal $\xi_1 = \xi_2$. We use dimensionless units: All energies are normalized to πT_c and the lengths on right/left are normalized to ξ_s^*/ξ_α. Separating the highest derivatives $\theta''_{\{s,\alpha\}}$, we can rewrite the Usadel equations as

$$\theta''_{\{s,\alpha\}} + \Delta_{\{s,\alpha\}} \cos\theta_{\{s,\alpha\}} - \omega \sin\theta_{\{s,\alpha\}} = 0. \tag{22}$$

This equation determines $\theta_{\{s,\alpha\}}$ as function of the discrete Matsubara frequency $\omega = t(2n+1)$ with $t = T/T_c$.

For simplicity, we neglect the intraband pairing interactions and consider only the repulsive interband coupling, parametrized by λ_{12} and λ_{21}. This is a reasonable approximation for the case of iron pnictides, in which the interband pair scattering is believed to be driving the superconductivity. Proper generalization, including the (attractive or repulsive) intraband terms, is straightforward. The self-consistency equation for Δ_α (8b) becomes

$$\Delta_\alpha = -2t\lambda_{\alpha\beta} \sum_{n=0}^{N_{\max}} \sin\theta_\beta, \tag{23}$$

with $\alpha,\beta = 1,2$ or $2,1$, the sum is over Matsubara frequencies, and $N_{\max} = \omega_{\max}/(2\pi T) - 1/2$, where $\omega_{\max}$ is some frequency cutoff.

The boundary conditions at the outside boundaries, $x = -d_s, d_\pm$, are $\theta'_s(-d_s) = 0$ and $\theta'_\alpha(d_\pm) = 0$. For the boundary conditions at the s-$s_\pm$ interface we obtain in the case of the aligned state (see Appendix B)

$$\theta'_s = \sum_\alpha \frac{\theta'_\alpha}{\gamma_\alpha}, \tag{24a}$$

$$\theta'_\alpha = \frac{1}{\gamma_{B\alpha}} \sin(\theta_\alpha - \theta_s). \tag{24b}$$

Let us now consider the case of strongly frustrated boundary when the TRSB state appears. The Green's functions are now essentially complex quantities: $\Phi_s = \omega \tan\theta_s e^{i\varphi_s}$ and $\Phi_\alpha = i\omega \tan\theta_\alpha e^{i\varphi_\alpha}$ (the factor i in the definition of Φ_α is for convenience). For the $s_\pm$ state we have $\varphi_1 - \varphi_2 = \pi$. Correspondingly, the s-wave gap and the two gaps of the order parameter can be written as $\Delta_s e^{i\chi_s}$ and $i\Delta_\alpha e^{i\chi_\alpha}$, where the (real) parameters $\Delta_{\{s,\alpha\}}$ and $\chi_{\{s,\alpha\}}$ have to be determined from the self-consistency equations.

The transformed Usadel equations for the highest derivatives $\theta''_{\{s,\alpha\}}$ and $\varphi''_{\{s,\alpha\}}$ in this case become

$$\varphi'' + 2\cot\theta\varphi'\theta' - \frac{\Delta}{\sin\theta}\sin(\varphi-\chi) = 0, \tag{25a}$$

$$\theta'' - \sin\theta\cos\theta(\varphi')^2 - \omega\sin\theta + \Delta\cos\theta\cos(\varphi-\chi) = 0, \tag{25b}$$

where, for brevity, we omitted the subscripts $\{s,\alpha\}$. We use the same normalization for all energies and lengths as in Eq. (22).

The self-consistency equation for Δ_α is

$$\Delta_\alpha e^{i\chi_\alpha} = -2t\lambda_{\alpha\beta} \sum_{n=0}^{N_{\max}} \sin\theta_\beta e^{i\varphi_\beta}. \tag{26}$$

This complex equation can be split into two real equations for Δ_α and χ_α:

$$\Delta_\alpha = 2t\lambda_{\alpha\beta}\left[\left(\sum_n \sin\theta_\beta\cos\varphi_\beta\right)^2 + \left(\sum_n \sin\theta_\beta\sin\varphi_\beta\right)^2\right]^{1/2},$$

$$\chi_\alpha = -\arctan\left(\sum_n \sin\theta_\beta\sin\varphi_\beta \Big/ \sum_n \sin\theta_\beta\cos\varphi_\beta\right).$$

The negative sign in the second equation—a straightforward consequence of the fact that $\lambda_{\alpha\beta}$ is repulsive—leads to somewhat counterintuitive result. The proximity effect tends to align the phases of Φ_s and Φ_α. Φ_α, in turn, determines the order parameter Δ_β through the self-consistency equation, which tends to make the phases difference between Φ_α and Δ_β close to π (to compensate for the "wrong" sign of the interaction). This means that, due to the proximity effect, the phase difference between Δ_α and Δ_s *increases* (measured from the positive axis), rather than decreases (see Fig. 1 for a pictorial presentation of this argument). This is a somewhat oversimplified picture, since φ_α depends on the Matsubara frequency. As can be seen from the Eqs. (8a) and (8b), for high frequencies the derivative term becomes unimportant and $\Phi_\alpha \to \Delta_\alpha$ meaning that $\varphi_\alpha \to \chi_\alpha$. This implies that φ_α changes its sign as a function of ω. To obtain Δ_β we have to sum over all n and this leads to "smearing" of the contributions to χ_β over a phase interval. Nonetheless, as we will see, the intuitive argument above seems to be qualitatively correct.

The boundary conditions at the outside boundaries are given by

$$\theta'_s(-d_s) = 0, \quad \varphi'_s(-d_s) = 0, \quad \theta'_\alpha(d_\pm) = 0, \quad \varphi'_\alpha(d_\pm) = 0.$$

The boundary conditions at the s-$s_\pm$ interface in θ parametrization are more complicated and we derive them in Appendix B. In reduced units these conditions are

$$\theta'_\alpha = -\frac{1}{\gamma_{B\alpha}}\left[\cos\theta_\alpha\sin\theta_s\sin(\varphi_s-\varphi_\alpha) - \cos\theta_s\sin\theta_\alpha\right], \tag{27a}$$

$$\varphi'_\alpha\sin\theta_\alpha = \frac{1}{\gamma_{B\alpha}}\sin\theta_s\cos(\varphi_s-\varphi_\alpha), \tag{27b}$$

$$\theta'_s = -\sum_\alpha \frac{1}{\tilde\gamma_{B\alpha}}\left[\cos\theta_\alpha\sin\theta_s + \cos\theta_s\sin\theta_\alpha\sin(\varphi_\alpha-\varphi_s)\right], \tag{27c}$$

$$\varphi'_s\sin\theta_s = \sum_\alpha \frac{1}{\tilde\gamma_{B\alpha}}\sin\theta_\alpha\cos(\varphi_\alpha-\varphi_s). \tag{27d}$$

To summarize, we have developed an entirely self-consistent scheme, based on Usadel equations and supplemented by the appropriate self-consistency equations and

boundary conditions. Unfortunately, due to its considerable complexity, in the general case it has to be solved numerically. To do this, we start with a guess for θ_s, θ_α, and φ_α, solve it on the $s_\pm$ side, using two of the boundary conditions at $x = 0$ and the boundary conditions at $x = d_\pm$, then write the third condition at $x = 0$ with the new solutions for θ_α, φ_α and use it to solve for θ_s. With such obtained solution we rewrite the two initially used boundary conditions and again solve for θ_α and φ_α. We repeat the process until self-consistency is achieved. To simplify the calculations, in some cases we expanded the equations around the bulk value $\theta_\alpha = \arctan(\Delta_{\alpha,0}/\omega)$, $\varphi_\alpha = 0$, where $\Delta_{\alpha,0}$ is the bulk gap for the α band.

Once calculations have produced self-consistent solutions of the equations on both sides of the boundary, we can obtain the DoS, $N_{\{s,\alpha\}}(E,x)$. For this, we rewrite the equations and boundary conditions with analytically continued frequency $i\omega \to E + i\delta$ and with computed gap functions $\Delta_s(x)$, $\Delta_\alpha(x)$ and solve them again for the real-energy Green's functions $\theta_{\{s,\alpha\}}(E,x)$. Once these equations are solved, the DoSs is given by Eq. (14) or, in the θ parametrization, by

$$N_{\{s,\alpha\}}(E,x) = \mathrm{Re}[\cos\theta_{\{s,\alpha\}}(E,x)].$$

In the following sections we review properties of the proximity system for different cases.

VI. ALIGNED STATE

With the formalism described in the Secs. III–V, we are now ready to study the proximity effects in several particular cases.

A. Identical $s_\pm$ bands

The aligned states appear when the bulk and boundary condition parameters are not symmetric with respect to the band indices interchange (asymmetric $s_\pm$ state). For simplicity, we first consider the asymmetry only in the coupling strength $\gamma_{B1} \neq \gamma_{B2}$, while keeping the rest of the parameters symmetric. In particular, this means that close to the boundary $|\Delta_1| \neq |\Delta_2|$, but in the bulk the symmetric $s_\pm$ state is restored and $\Delta_2 = -\Delta_1$ (see right middle panel of Fig. 1). In all numerical calculations presented in this section, unless stated otherwise, we fixed several parameters: $d_\pm = 8\xi_\alpha$, $T_c^s = 0.222T_c$, $T = 0.1T_c$. The choice of T_c^s gives relation for the gap $\Delta_s^{\mathrm{bulk}}/(\pi T_c) = 0.1213$. Other parameters which enter the calculations are specified in the figure captions.

Since in a way the aligned state is closer to a conventional multiband superconductor than the TRSB state is, we expect the usual positive proximity effect to be predominant. Indeed, as we will see, the s-wave superconductor's gap tends to be *enhanced* by the presence of the stronger $s_\pm$ superconductor (which in turn is suppressed). This is easy to understand when the s-wave gap is much stronger coupled to one of the gaps on the $s_\pm$ side, since this case can be thought as proximity between two single-band superconductors. Coupling to the other gap on the $s_\pm$ side can be treated as a small perturbation. However, when the interboundary couplings are close, and the system is strongly frustrated (and thus close to the TRSB state), the proximity effect turns negative, with all superconducting gaps suppressed close to the $x = 0$ plane. Therefore, the "sign" of the proximity effect on the s-wave side in the aligned state is not universal and depends on both bulk and boundary properties of the materials.

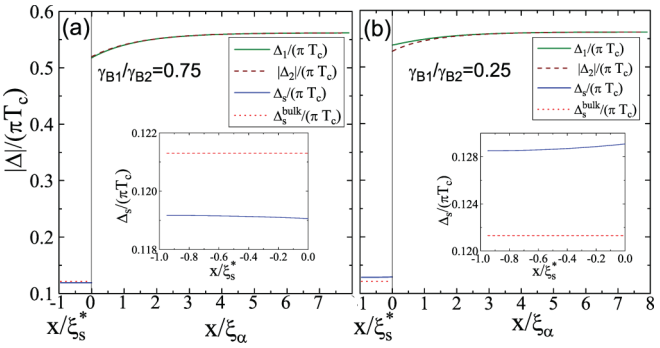

FIG. 4. (Color online) These plots illustrate behavior of the gaps in the proximity sandwich for two values of the ratio γ_{B1}/γ_{B2}. The insets show magnifications of $\Delta_s(x)$ and, for comparison, Δ_s^{bulk} is also shown. Other used parameters are $\gamma_{B1} = 10$, $d_s = \xi_s^*$, and $\gamma_\alpha = 10$. One can see that for weakly asymmetric coupling $\gamma_{B1}/\gamma_{B2} = 0.75$ in plot (a) the proximity effect is negative [$\Delta_s(x) < \Delta_s^{\mathrm{bulk}}$], while for strongly asymmetric coupling $\gamma_{B1}/\gamma_{B2} = 0.25$ in the plot (b) the proximity effect becomes positive [$\Delta_s(x) > \Delta_s^{\mathrm{bulk}}$].

On Fig. 4 we illustrate this effect by showing calculations of $\Delta_s(x)$ for two different values of γ_{B1}/γ_{B2} (we change γ_{B2} while keeping all other parameters of the system fixed). As can be seen, Δ_s is enhanced or suppressed close the interface [corresponding to a sign change of $\theta_s'(0)$], depending on the ratio of the boundary transparencies. Note that the transition between the two cases coincides with change of the ratio of $\Delta_1(0)/|\Delta_2(0)|$. For positive (negative) proximity effect this ratio is larger (smaller) than 1. This is easy to understand from the first condition in Eq. (24a); it is clear that (for $\gamma_1 = \gamma_2$) the sign of θ_s' is determined by the $\theta_1' + \theta_2'$. Also remember that Δ_1 is determined by θ_2 and vice versa in the interband coupling model.

Now we proceed to systematically study the interplay between the different physical parameters and the transition from negative to positive proximity effects. We plot in Fig. 5(a) the value of $\Delta_s(-d_s)$ and $\Delta_s(0)$ as a function of the ratio γ_{B1}/γ_{B2} (the model, of course, is symmetric with respect to the exchange $\gamma_{B1} \leftrightarrow \gamma_{B2}$). Δ_s is suppressed as this ratio gets closer to one (and the frustration increases), in agreement with our previous qualitative arguments and analytical calculations. With increasing the ratio the proximity effect turns from positive to negative when the ratio γ_{B1}/γ_{B2} exceeds the critical value $\approx$0.578. The linear approximation for the average correction to the s-wave gap (17) in the case $|\Delta_{20}| = \Delta_{10}$ gives the following estimate for this critical value, $\gamma_{B1}/\gamma_{B2} \approx (\Delta_{10} - \Delta_{s0})/(\Delta_{10} + \Delta_{s0})$. For our parameters this gives $\gamma_{B1}/\gamma_{B2} \approx 0.645$ which somewhat exceeds the value obtained in numerical calculations. As the system gets closer to the line of maximal frustration $\gamma_{B1} = \gamma_{B2}$ it eventually undergoes a phase transition to the TRSB state.

In Figs. 5(b) and 5(c) we illustrate the dependence of the gap parameters on the coupling strength $1/\gamma_{B1}$ for fixed ratio $\gamma_{B2}/\gamma_{B1} = 2$. At small coupling strength, $1/\gamma_{B1} \lesssim 0.07$ the behavior of all gaps agrees with the linear approximation described in Sec. IV. At larger coupling the s-wave gap

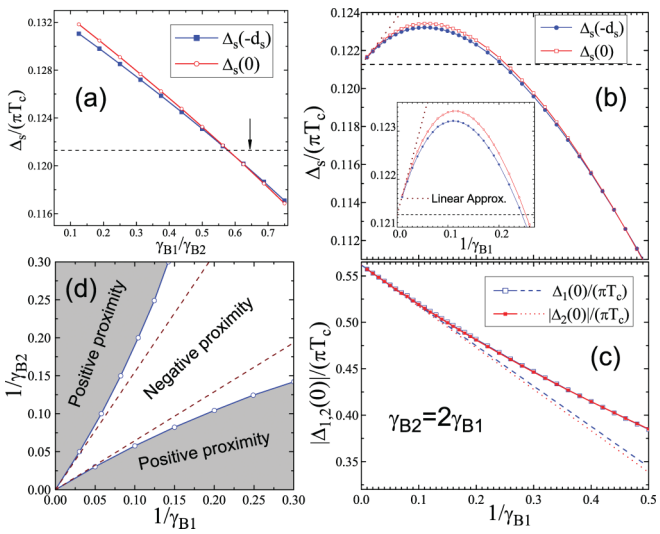

FIG. 5. (Color online) (a) Plot of $\Delta_s(-d_s)$ and $\Delta_s(0)$ as a function of the ratio γ_{B1}/γ_{B2}. As γ_{B1}/γ_{B2} approaches 1, the enhancement on the s-wave side is replaced with suppression (the proximity effect changes from positive to negative). The arrow indicates the expected location of the transition to the negative proximity from the weak-coupling approximation, $\gamma_{B1}/\gamma_{B2} \approx 0.645$. (b),(c) The dependencies of the s-wave gap parameter at the boundaries [plot (b)] and the $s_\pm$ gaps at the interface [plot (c)] on the coupling strength with the first band, $1/\gamma_{B1}$ for fixed ratio $\gamma_{B2}/\gamma_{B1} = 2$. The inset in the plot (b) blows up the small-coupling region. Behavior of the gaps expected from the linear approximation is also shown [the dotted line in the plot (b) and the dashed and dotted lines in the plot (c)]. (d) The regions of the negative and positive proximity in the $1/\gamma_{B1}$-$1/\gamma_{B2}$ plane obtained by numerical calculations. The dashed lines show boundaries obtained within weak-coupling approximation. Parameters used in the calculation for all plots are $\gamma_{B1} = 10$, $\gamma_\alpha = 10$, $d_s = \xi_s^*$.

strongly deviates from the linear approximation. In particular, it reaches maximum at some value of coupling and decreases at larger values. With further increase of coupling, Δ_s drops below the bulk value; that is, proximity becomes negative. Qualitatively, this behavior can be understood as follows: The positive and negative contributions to Δ_s are roughly proportional to $\Delta_1(0) - \Delta_s$ and $|\Delta_2(0)| + \Delta_s$ correspondingly. As the $s_\pm$ gap parameters reduce and become closer to the s-wave gap with increasing coupling, the negative term becomes relatively stronger. Another notable property is that the absolute values of the $s_\pm$ gap parameters Δ_1 and $|\Delta_2|$ remain very close, in spite of significant asymmetry in coupling strength.

In Fig. 5(d) we show the regions of the negative and positive proximity in the coupling-strengths plane obtained by numerical calculations and compare them with predictions of the weak-coupling approximation. In agreement with the plots 5(a)–5(c), we can see that stronger coupling favors negative proximity meaning that the weak-coupling approach underestimates the width of the negative-proximity region for small $\gamma_{B\alpha}$.

Unfortunately, there is no obvious way to control the coupling parameters $\gamma_{B\alpha}$. One parameter which can be varied relatively easily in experiment is the thickness of the layers.

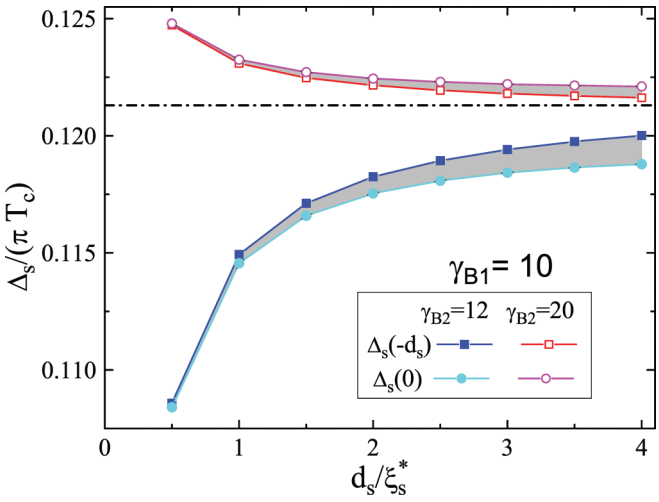

FIG. 6. (Color online) Plot of $\Delta_s(-d_s)$ and $\Delta_s(0)$ as a function of d_s for $\gamma_{B1} = 10$ and two values of γ_{B2}, 12 and 20, corresponding to negative and positive proximity effect. As the thickness increases $\Delta_s(-d_s)$ approaches its bulk value.

In Fig. 6 we show the Δ_s as a function of d_s for $\gamma_{B1} = 10$ and two values of γ_{B2}, 12 and 20, corresponding to negative and positive proximity effect. There are two natural tendencies which can be observed. First, with increase of d_s the value of Δ_s increases (decreases) for the positive (negative) proximity. Second, the difference between $\Delta_s(0)$ and $\Delta_s(-d_s)$ increases with thickness until it finally saturates for $d_s \gg \xi_s$.

In this section we demonstrated that both negative and positive proximity effects may present close to s-$s_\pm$ interfaces for the aligned state. The sign of the proximity effect is determined by nontrivial interplay of the physical parameters in the system. In general, negative proximity effect is expected in the region around the line which separates the aligned and the TRSB states, for intermediate frustration of the interface.

B. Nonequal $s_\pm$ gaps

In this section we present numerical results illustrating properties of aligned state when the bulk gaps of $s_\pm$ superconductor have different magnitudes. This situation is probably more typical and has one definite practical advantage with respect to the case of identical or close $s_\pm$ gaps: Different gaps induce features into the s-wave DoS which are well separated in energy and thus easier to detect experimentally. Therefore, in this section, in addition to the behavior of the gaps, we also study behavior of DoSs. We investigate in detail the shapes of DoS features and their sensitivity to the coupling parameters.

We first consider the case of weak coupling (large $\gamma_{B\alpha}$ and $\tilde{\gamma}_{B\alpha}$) and compare numerical calculations with the analytical results presented of Sec. IV. In particular, this allows us to evaluate limits of the weak-coupling approximation. Figure 7 illustrates behavior of the gaps for different coupling strengths. For an $s_\pm$ superconductor we consider again the interband coupling model and the gap values are fixed by the coupling constants which we take as $\lambda_{12} = -0.4$ and $\lambda_{21} = -0.2$ giving the bulk gaps $|\Delta_{10}| = 0.683$ and $|\Delta_{20}| = 0.456$ (in units of πT_c). We assume $t_{cs} = T_c^s/T_c = 0.3$ giving $\Delta_{s0} = 0.1675$. We again assume identical coherence lengths for two $s_\pm$

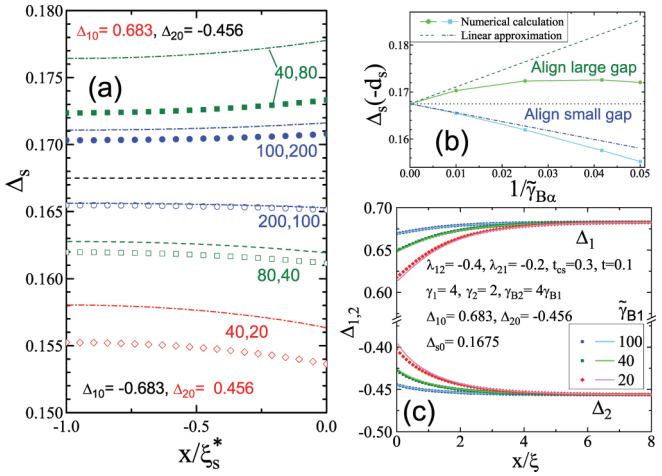

FIG. 7. (Color online) (a) The coordinate dependences of the s-wave order parameter Δ_s for different couplings to the $s_\pm$ bands. The plots are labeled by $\tilde{\gamma}_{B1}, \tilde{\gamma}_{B2}$. Other parameters are listed in plot (c). The horizontal dashed line shows the bulk gap. The curves above this line (positive proximity) correspond to the alignment with the large gap, Δ_1, while the curves below this line (negative proximity) correspond to the alignment with the small gap, Δ_2. Three dot-dashed lines above and three dashed lines below show analytical predictions based on linear approximation [Eq. (15b)]. (b) The dependences of the s-wave gap at the outside boundary on the coupling strength with the aligned gap $1/\tilde{\gamma}_{B\alpha}$; dashed lines show linear approximations. (c) The coordinate dependences of the $s_\pm$-wave order parameters for the alignment with the larger gap. The solid lines show the linear approximation.

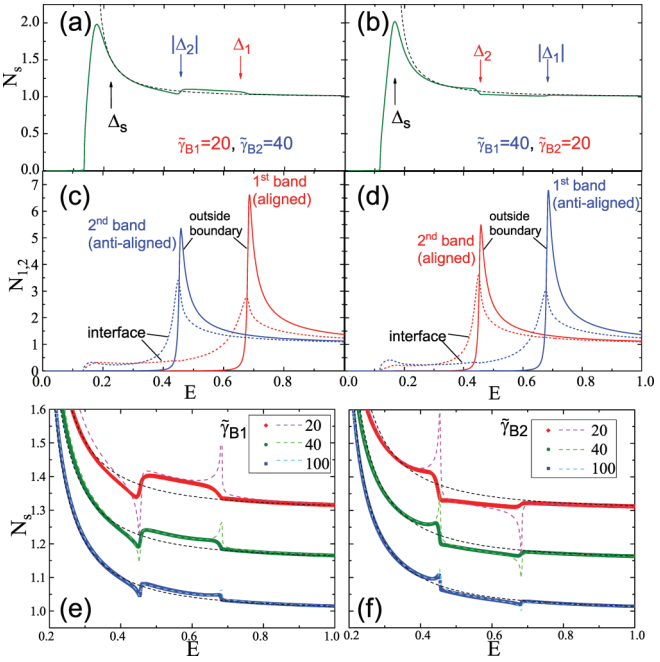

FIG. 8. (Color online) Behavior of the densities of states for the same parameters as in Fig. 7. Plots (a) and (b) illustrate shapes of s-wave DoS for the cases when the s-wave order parameter is aligned with large and small gap correspondingly for the strongest used coupling strength. The dashed lines show the BCS density of states. Plots (c) and (d) show the partial DoS for two $s_\pm$ bands at the interface and at the outside boundary for these two cases. Plots (e) and (f) demonstrate the evolution of the feature in the s-wave DoS with varying strength of coupling. The plots are displaced vertically for clarity. The dashed lines show predictions of the linear approximation.

bands. Due to relation (13), we have $\gamma_1/\gamma_2 = \lambda_{12}/\lambda_{21} = 2$ and therefore we select $\gamma_1 = 4$, $\gamma_2 = 2$. All parameters used in these calculations are listed in Fig. 7(c). We consider both cases of alignment of the s-wave gap Δ_s with large gap Δ_1 ($\Delta_s \uparrow\uparrow \Delta_1$) and with small gap Δ_2 ($\Delta_s \uparrow\uparrow \Delta_2$). We only vary coupling strengths $\propto 1/\tilde{\gamma}_{B\alpha}$ preserving the ratio $\tilde{\gamma}_{B2}/\tilde{\gamma}_{B1} = 2$ for $\Delta_s \uparrow\uparrow \Delta_1$ and $\tilde{\gamma}_{B1}/\tilde{\gamma}_{B2} = 2$ for $\Delta_s \uparrow\uparrow \Delta_2$.

Figure 7(a) shows the coordinate dependences of the s-wave order parameter. The symbols show numerical results and the lines show analytical results in the linear order with respect to $1/\tilde{\gamma}_{B\alpha}$ based on Eq. (15b). The bulk gap is shown by the dashed line. For selected parameters, the alignment with the large gap corresponds to positive proximity, while the alignment with the small gap corresponds to negative proximity. We can see that the linear approximation accurately describes behavior of Δ_s only for weakest coupling $\tilde{\gamma}_{B(1,2)} = 100$. It always overestimates the gap parameters and breaks down already for rather weak coupling strength. This is even clearer on Fig. 7(b), where the gap parameter at the outside surface is plotted versus the coupling strength with the aligned gap. Deviations are especially large in the case of alignment with the large gap. The found nonmonotonic dependence of Δ_s is similar to the case of identical $s_\pm$ gaps shown in Fig. 5(b).

Figure 7(c) shows the coordinate dependences of the $s_\pm$ gaps in the case $\Delta_s \uparrow\uparrow \Delta_1$. As expected, both gaps are suppressed at the interface. This suppression grows with increasing coupling strength, and disappears away from the boundary for a distance of the order of the coherence length. Behavior for the case $\Delta_s \uparrow\uparrow \Delta_2$ is very similar. It is peculiar that, in contrast to the s-wave gap, the linear approximation accurately describes the behavior of the $s_\pm$ gap parameters in the whole studied range of parameters.

Figure 8 illustrates behavior of the DoS for the same set of parameters. Figures 8(a) and 8(b) demonstrate full shapes of the s-wave DoS at $x = -d_s$, $N_s(E)$, for the cases $\Delta_s \uparrow\uparrow \Delta_1$ and $\Delta_s \uparrow\uparrow \Delta_2$ correspondingly and for strongest coupling in this series. Interaction with the $s_\pm$ superconductor induces specific features in the s-wave DoS near the energies of $s_\pm$ gaps. Figures 8(e) and 8(f) show evolution of these s-wave DoS features with increasing coupling strength. The weak-coupling approximation for the case of thin s-superconductor layer [Eq. (21)] suggests that the aligned and antialigned gaps should induce a small peak and a dip, correspondingly.[47] For comparison, the analytical weak-coupling results are also shown in Figures 8(e) and 8(f) by dashed lines. We can see that the analytical approximation describes well the shapes of correction except the regions close to the $s_\pm$ gaps where it overestimates the amplitudes of peaks and dips. Nevertheless, small asymmetric peaks and dips do appear for weak coupling strength, in agreement with analytical predictions. These peaks and dips are rapidly smeared with increasing coupling strength. Equation (21) also suggests that the correction is strongly asymmetric: The s-wave DoS is only enhanced or reduced for $E < |\Delta_\alpha|$. This steplike behavior of the correction is indeed

seen in Figs. 8(a) and 8(b) and, in more detail, in Figs. 8(e) and 8(f). In fact, with increasing coupling the peaks and dips evolve into smooth up and down steps. The amplitude of this steplike feature between $|\Delta_2|$ and $|\Delta_1|$ monotonically increases with increasing coupling and its shape is well described by the analytical approximation.

Figures 8(c) and 8(d) show partial DoSs for two $s_\pm$ bands at the interface and at the outside boundary. Coupling with an s-wave superconductor leads to considerable smearing of the DoS peaks at the interface. The most prominent feature is the appearance of the tails spreading down to the s-wave spectral gap. This is a well-known feature which is always induced in a superconductor by proximity with either metal or weaker superconductor.[60] Note also that the peaks positions for DoS at the interface do not shift much with respect the bulk gap values. There is no qualitative difference in the DoS shapes between the aligned and antialigned bands.

We also studied the evolution of the proximity properties with varying the partial resistances for two $s_\pm$ bands, while keeping fixed the total boundary resistance. As the total boundary *conductance* $\Sigma_B = 1/R_B$ is equal to sum of the partial boundary conductances $1/R_{B\alpha} \propto 1/\tilde{\gamma}_{B\alpha}$, the total boundary resistance can be set by fixing $1/\tilde{\gamma}_B = 1/\tilde{\gamma}_{B1} + 1/\tilde{\gamma}_{B2}$. We select this parameter as $1/\tilde{\gamma}_B = 0.15$ corresponding to the moderately strong coupling strength. All other parameters are the same as in Fig. 7. Figure 9 illustrates evolution of the s-wave order parameter and DoS for varying partial resistances for two bands. The plots are marked by the pair $\tilde{\gamma}_{B1}, \tilde{\gamma}_{B2}$. We can see that for strongly asymmetric coupling proximity effect is positive, there is pronounced BCS peak near the bulk gap, and pronounced steplike features at the $s_\pm$ gaps. The step amplitude is typically larger for a smaller gap. As coupling becomes more symmetric, the proximity

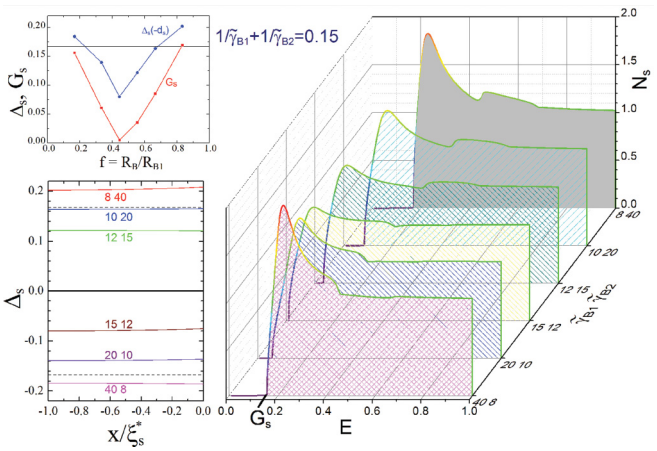

FIG. 9. (Color online) Evolution of the s-wave for the order parameter (left lower plot) and DoS (left plot) for the fixed total boundary resistance set by condition $1/\tilde{\gamma}_{B1} + 1/\tilde{\gamma}_{B2} = 0.15$ and for varying partial resistances for two bands. Coupling to the larger gap in the right plot progressively increases from the back to the front plot. Plots are marked by $\tilde{\gamma}_{B1}$, $\tilde{\gamma}_{B2}$. Other parameters are the same as in the previous plots. The upper left plot shows the order parameter at the outside boundary and the gap in spectrum (defined in the right plot) as a function of a fraction of the first-band conductance with respect to the total conductance through the boundary.

turns negative, the BCS peak smears, and the amplitudes of the proximity-induced features decrease. Also, the gap in the spectrum corresponding to vanishing of DoS, G_s, rapidly decreases as coupling becomes more symmetric. This is seen more clearly in the upper left plot where the order parameter and spectral gap are plotted as function of a fraction of the first-band conductance with respect to the total conductance, $f = R_B/R_{B1}$. Both parameters have quite sharp cusplike dependence on f and the spectral gap practically vanishes in the minimum. Note that, in contrast to the BCS DoS, the spectral gap is significantly smaller than the order parameter.

In the next section we consider behavior of the order parameter for the TRSB state.

VII. TRSB STATE

For illustration we consider here only the simplest TRSB state, in the case the two-gap superconductor has identical bands, coupled symmetrically to the s-wave layer (see the panel at the right upper corner of Fig. 1). The symmetry simplifies the calculations considerably. This is also the case which favors the TRSB state most, since the frustration at the interface is the strongest possible.

Due to the symmetry of the problem we can choose $\Phi_s(0)$ to be real. In this case $\Phi_1^* = \Phi_2$ and we can write $\Phi_1 = i\omega \tan\theta e^{i\varphi}$, $\Phi_2 = -i\omega \tan\theta e^{-i\varphi}$. However, to preserve the uniformity in notation we keep the (now redundant) α indexing; $\varphi_1 = -\varphi_2 = \varphi$, $\theta_1 = -\theta_2 = \theta$. The above implies, of course, that we can write the gap functions as $\Delta_1 = \Delta e^{i\chi}$, $\Delta_2 = -\Delta e^{-i\chi}$. φ and χ parametrize the deviation from the $s_\pm$ state and we expect that in the bulk $\varphi \to 0$ and Φ_1, Φ_2 become purely imaginary. From the boundary conditions it is clear that Φ_s can be chosen real everywhere [both $\mathrm{Im}(\Phi_s(0)] = \mathrm{Im}[\Phi_s'(0)] = 0$—no imaginary component develops). In the θ parametrization the s-wave Green's function is again determined by Eq. (22). The equations for the $s_\pm$ side are identical to Eqs. (25b), but there are now only two independent variables (instead of four). In this case, the boundary conditions (V) can be simplified as

$$\theta_\alpha' = \frac{1}{\gamma_{B\alpha}}(\sin\theta_s \cos\theta_\alpha \sin\varphi_\alpha + \cos\theta_s \sin\theta_\alpha),$$

$$\varphi_\alpha' = \frac{1}{\gamma_{B\alpha}} \sin\theta_s \csc\theta_\alpha \cos\varphi_\alpha,$$

$$\theta_s' = -\frac{2}{\gamma_\alpha \gamma_{B\alpha}} \cos\theta_s \sin\theta_\alpha (\tan\theta_s \cot\theta_\alpha + \sin\varphi_\alpha).$$

We proceed to solve the equations numerically. In Fig. 10 we show the results of calculation for Δ, χ (we again remind the reader that $\Delta_2 = -\Delta_1$, $\chi_2 = -\chi_1$), and Δ_s done for different values of $\gamma_{B\alpha}$. Several things should be noted. First, $\chi(x)$ is positive and thus the $s_\pm$ gaps are pushed away from Δ_s, in accordance with the argument in Sec. III. Second, several ξ_α away from the boundary, χ becomes very small and the order parameter returns to its $s_\pm$ bulk form (since the TRSB state exists because the frustration created by the boundary). Third, decreasing $\gamma_{B\alpha}$ (increasing the boundary transparency) tends to reduce both $\Delta_\alpha(0)$ and $\Delta_s(0)$, and increase $\chi(0)$, as expected. It is important to note that decreasing $\gamma_{B\alpha}$ pushes $\Delta_s(x)$ down

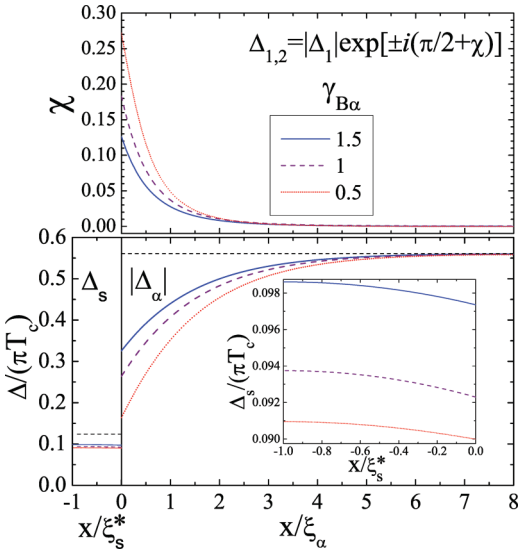

FIG. 10. (Color online) Behavior of the order parameters in the symmetric TRSB state for three different boundary transparency parameters $\gamma_{B\alpha}$ and for $\gamma_\alpha = 5$. The rest of the parameters are given in the text. The bottom plots show the coordinate dependencies of the absolute values of the order parameters and top plot shows the phase $\chi(x)$ of the $s_\pm$ order parameter. χ goes to zero in the bulk, where the state is $s_\pm$, with phase rotated by $\pi/2$ with respect to the s-wave order parameter. Note that $|\Delta_1(0)|$ and Δ_s decrease and the value of $\chi(0)$ increases with the increase of the interface transparency.

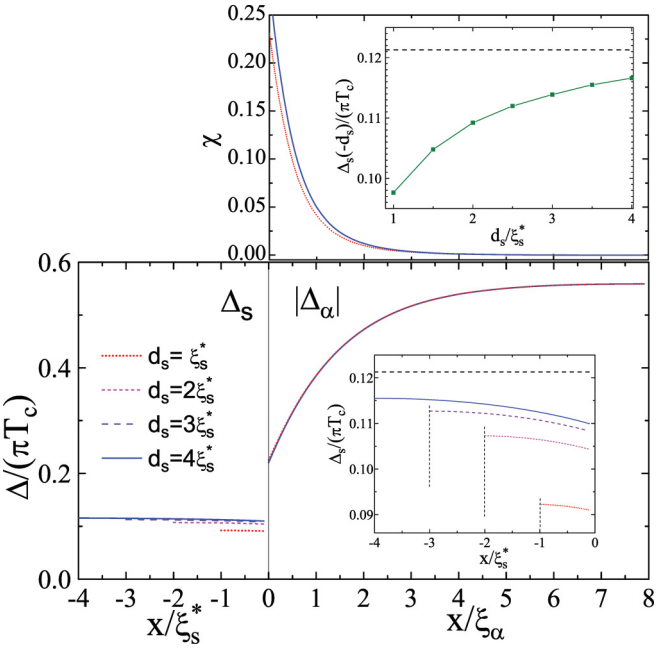

FIG. 11. (Color online) $\Delta(x)$, $\chi(x)$, and $\Delta_s(x)$ for $\gamma_\alpha = 5, \gamma_{B\alpha} = 0.75$ and four different values of d_s. The changes on the right side are generally quite small. In contrast, $\Delta_s(x)$ is suppressed noticeably for thin films. This is more clearly seen in the bottom inset, which shows the magnified plots of $\Delta_s(x)$. The top inset shows the d_s dependence of the Δ_s at the outer surface.

everywhere, while keeping its general shape intact [unlike the changes of $\Delta_\alpha(x)$]. This is due to the relative thinness of the s-wave layer.

Since controlling the interface parameters $\gamma_{B\alpha}$ is not easy experimentally, we also study evolution with increasing thickness of the s-wave superconductor, d_s, for the same parameters of the interface. We vary the thickness of the s-wave layer from ξ_s^* to $4\xi_s^*$ and show the results of the calculation on Fig. 11. On the $s_\pm$ side the changes are modest; χ shifts a bit, while Δ_α is virtually unchanged for different d_s. Note that as d_s decreases, the gap on the right side gets slightly closer to the bulk $s_\pm$ state (χ goes down). The changes on the other side are more pronounced. Δ_s is always suppressed as $x \to 0$, but, as in the previous case, Δ_s is significantly below its bulk value *everywhere*.

These results are summarized in the upper inset of Fig. 11 where we plot the value of the gap on the external left boundary as a function of the s-wave layer thickness. We see the result of the negative proximity effect as a suppression of $\Delta_s(-d_s)$ for thinner films. With the increase of the film thickness $\Delta_s(-d_s)$ goes up, however, it stays noticeably below its bulk value even for $d_s = 4\xi_s^*$.

We can see that accurate numerical computations confirm the structure of the TRSB state expected from general considerations. In particular, in the TRSB state the negative proximity effect is present and, depending on the precise values of various physical parameters, can be quite pronounced.

VIII. DISCUSSION AND CONCLUSIONS

One important point should be addressed before we apply our conclusions to structures involving iron-based superconductors. These materials have quite short coherence length and are likely in the clean limit. In conventional superconductors there is smooth interpolation between the clean and the dirty limit and results obtained by solving the Usadel equations are expected to be qualitatively or even quantitatively correct in the clean limit.[61] Furthermore, the boundary itself acts as a scatterer and can push the region up to several ξ away in the dirty regime. This again justifies the use of the Usadel equations. In $s_\pm$ superconductors the situation is much less clear; because of the unconventional nature of the order parameter interband impurity scattering is pair-breaking. If strong, it can completely destabilize the $s_\pm$ state.[62] However, if this scattering channel can be neglected, as we have done (so $s_\pm$ is stable even close to the interface), then our approach should provide a reasonably good description. Whether this can be justified in realistic experimental situations is unclear, at least at the moment.

In conclusion, we have studied the proximity effects close to a boundary between s and $s_\pm$ superconductors. Based on frustrated Josephson junction model, we have suggested phase diagram for such system. Because of the frustration, present at such interface, several interesting phenomena are possible. In the case of maximum frustration—when the coupling of the two gaps on the $s_\pm$ side with the s-wave superconductor is comparable—a state which breaks time-reversal symmetry appears. Such a superconducting state is also characterized by a negative proximity effect, because of the frustration the

gap amplitudes on both sides are suppressed. In the case of significant asymmetry in the inter-boundary coupling the aligned $s_\pm$ can be stabilized even close to the interface. Interestingly, such an aligned state may also lead to negative proximity effect. It is very important to note that this effect is unique to the s-$s_\pm$ structures and is not present close to a conventional s-s_{++} boundary. Observation of such an effect in structures with iron pnictides/chalcogenides will be a definitive proof that their order parameter belongs to the unconventional $s_\pm$ class. Another unique fingerprint of this order parameter is that it induces a negative feature in the s-wave DoS.

ACKNOWLEDGMENTS

We acknowledge useful discussions with Thomas Proslier, Alex Levchenko, Laura Greene, Dale Van Harlingen, and James Eckstein. This work was supported by UChicago Argonne, LLC, operator of Argonne National Laboratory, a US Department of Energy Office of Science laboratory, operated under Contract No. DE-AC02-06CH11357, and by the "Center for Emergent Superconductivity," an Energy Frontier Research Center funded by the US Department of Energy, Office of Science, Office of Basic Energy Sciences under Award No. DE-AC0298CH1088.

APPENDIX A: BOUNDARY-INDUCED CORRECTIONS IN THE WEAK-COUPLING LIMIT FOR THE ALIGNED STATE

In this Appendix we consider weak-coupling case $\gamma_{B\alpha} \gg 1$ and derive corrections to the Green's functions and gap parameter for aligned state in the linear order with respect to the coupling parameters $1/\gamma_{B\alpha}$.

1. s-wave superconductor

The first-order corrections to the s-wave Green's functions $\tilde{\Phi}_s$ and gap $\tilde{\Delta}_s$ obey the following equations:

$$\xi_{s,\omega}^2 \tilde{\Phi}_s'' - \tilde{\Phi}_s = -\tilde{\Delta}_s, \tag{A1a}$$

$$\lambda_s 2\pi T \sum_{\omega>0} \frac{\omega^2 \tilde{\Phi}_s}{\left(\omega^2+\Delta_s^2\right)^{3/2}} = \tilde{\Delta}_s, \tag{A1b}$$

with $\xi_{s,\omega}^2 = D_s/(2\sqrt{\omega^2+\Delta_s^2}) = \xi_{s,\Delta}^2(\Delta_s/\sqrt{\omega^2+\Delta_s^2})$ and $\xi_{s,\Delta}^2 = D_s/(2\Delta_s)$. In the boundary condition we can neglect the difference between Φ's and Δ's and approximate Δ's by their bulk values. This gives

$$\xi_s^* G_s \tilde{\Phi}_s' = -\sum_\alpha \frac{G_\alpha}{\tilde{\gamma}_{B\alpha}}(\Delta_s - \Delta_\alpha) \tag{A2}$$

at $x=0$ with $\tilde{\gamma}_{B\alpha} \equiv \gamma_\alpha \gamma_{B\alpha}$. The self-consistency condition also can be rewritten as

$$2\pi T \sum_{\omega>0}\left[\frac{\omega^2\tilde{\Phi}_s}{\left(\omega^2+\Delta_s^2\right)^{3/2}} - \frac{\tilde{\Delta}_s}{\omega}\right] + \tilde{\Delta}_s \ln\frac{T_c^s}{T} = 0. \tag{A3}$$

We split $\tilde{\Phi}_s$ into the two contributions, $\tilde{\Phi}_s = \tilde{\Phi}_{s,b} + \tilde{\Phi}_{s,\Delta}$, where $\tilde{\Phi}_{s,b}$ is induced by the boundary condition and $\tilde{\Phi}_{s,\Delta}$ is induced by the gap correction. The first contribution $\tilde{\Phi}_{s,b}$ can be found from the following equation and the boundary condition

$$\xi_{s,\omega}^2 \tilde{\Phi}_{s,b}'' - \tilde{\Phi}_{s,b} = 0, \tag{A4a}$$

$$\xi_s^* G_s \Phi_{s,b}' = -\sum_\alpha \frac{G_\alpha}{\tilde{\gamma}_{B\alpha}}(\Delta_s - \Delta_\alpha), \tag{A4b}$$

while the second contribution $\tilde{\Phi}_{s,\Delta}$ obeys the following equation and the boundary condition

$$\xi_{s,\omega}^2 \tilde{\Phi}_{s,\Delta}'' - \tilde{\Phi}_{s,\Delta} = -\tilde{\Delta}_s, \tag{A5a}$$

$$\xi_s^* G_s \Phi_{s,\Delta}' = 0. \tag{A5b}$$

The solution $\tilde{\Phi}_{s,b}(x)$ of the linear equation (A4a) with the boundary condition $\tilde{\Phi}_{s,b}' = 0$ at $x = -d_s$ is given by

$$\tilde{\Phi}_{s,b}(x) = C_{s,b}\cosh\left(\frac{x+d_s}{\xi_{s,\omega}}\right), \tag{A6}$$

where the constant $C_{s,b}$ can be found from the boundary condition at $x=0$,

$$C_{s,b} = -\frac{\xi_{s,\omega}/\xi_s^*}{\sinh(d_s/\xi_{s,\omega})}\sum_\alpha \frac{G_\alpha}{\tilde{\gamma}_{B\alpha}G_s}(\Delta_s - \Delta_\alpha).$$

We compute $\tilde{\Phi}_{s,\Delta}$ and $\tilde{\Delta}_s$ using the Fourier expansion, $\tilde{\Phi}_{s,\Delta} = \sum_{m=0}^\infty \tilde{\Phi}_{s,\Delta,m}\cos k_m x$, $\tilde{\Delta}_s = \sum_{m=0}^\infty \tilde{\Delta}_{s,m}\cos k_m x$, with $k_m = m\pi/d_s$. For $\tilde{\Phi}_{s,b}(x)$ [Eq. (A6)], the Fourier components $\tilde{\Phi}_{s,b,m}$ can be computed explicitly:

$$\tilde{\Phi}_{s,b,m} = -\frac{(2-\delta_m)\xi_{s,\omega}^2/(d_s\xi_s^*)}{1+\xi_{s,\omega}^2 k_m^2}\sum_\alpha \frac{\sqrt{\omega^2+\Delta_s^2}}{\sqrt{\omega^2+\Delta_\alpha^2}}\frac{\Delta_s-\Delta_\alpha}{\tilde{\gamma}_{B\alpha}}. \tag{A7}$$

Equation (A5a) immediately gives the following relation between the Fourier components $\tilde{\Phi}_{s,\Delta,m}$ and $\tilde{\Delta}_{s,m}$:

$$\tilde{\Phi}_{s,\Delta,m} = \frac{\tilde{\Delta}_{s,m}}{1+\xi_{s,\omega}^2 k_m^2}. \tag{A8}$$

Substituting this result into the self-consistency condition (A1b), we express $\tilde{\Delta}_{s,m}$ via $\tilde{\Phi}_{s,b,m}$

$$\tilde{\Delta}_{s,m} = \left\{2\pi T\sum_{\omega>0}\frac{\Delta_s^2+\omega^2\frac{\xi_{s,\omega}^2 k_m^2}{1+\xi_{s,\omega}^2 k_m^2}}{\left(\omega^2+\Delta_s^2\right)^{3/2}}\right\}^{-1} \times 2\pi T\sum_{\omega>0}\frac{\omega^2\tilde{\Phi}_{s,b,m}}{\left(\omega^2+\Delta_s^2\right)^{3/2}}. \tag{A9}$$

Equations (A7)–(A9) provide a complete solution of the problem.

For convenient comparison with the numerical calculations, we also present these results in the reduced form in which d_s is measured in units of $\xi_s^* = D_s/(2\pi T_c)$

and energies (ω, Δ's and Φ's) in units of πT_c:

$$\tilde{\Delta}_{s,m} = \left\{ 2t \sum_{\omega>0} \frac{1}{\left(\omega^2+\Delta_s^2\right)^{3/2}} \left[\Delta_s^2 + \omega^2 \frac{(\pi m/d_s)^2}{\sqrt{\omega^2+\Delta_s^2}+(\pi m/d_s)^2} \right] \right\}^{-1} \times 2t \sum_{\alpha,\omega>0} \frac{\omega^2}{\left(\omega^2+\Delta_s^2\right)\sqrt{\omega^2+\Delta_\alpha^2}} \frac{(2-\delta_m)/d_s}{\sqrt{\omega^2+\Delta_s^2}+(\pi m/d_s)^2} \frac{\Delta_\alpha-\Delta_s}{\tilde{\gamma}_{B\alpha}}, \tag{A10}$$

$$\tilde{\Phi}_{s,m} = \frac{1}{1+(\pi m/d_s)^2/\sqrt{\omega^2+\Delta_s^2}} \left(\tilde{\Delta}_{s,m} + \frac{2-\delta_m}{d_s} \sum_\alpha \frac{1}{\sqrt{\omega^2+\Delta_\alpha^2}} \frac{\Delta_\alpha-\Delta_s}{\tilde{\gamma}_{B\alpha}} \right), \tag{A11}$$

with $t = T/T_c$ and $\omega = 2t(n+1/2)$. At low temperatures the summation with respect to the Matsubara frequencies can be replaced by the integration $2\pi T \sum_{\omega>0} \to \int_0^\infty d\omega$. In this limit we can obtain an analytical result for the average correction to the order parameter, $\tilde{\Delta}_{s,0}$,

$$\frac{\tilde{\Delta}_{s,0}}{\pi T_c} = \frac{\xi_s^*}{d_s} \sum_\alpha U(\Delta_s/|\Delta_\alpha|) \frac{\Delta_\alpha-\Delta_s}{\tilde{\gamma}_{B\alpha}|\Delta_\alpha|},$$

$$\text{with} \quad U(a) = \int_0^\infty dz \frac{z^2}{\left(z^2+1\right)^{3/2}\sqrt{a^2z^2+1}} = \frac{K(1-a^2)-E(1-a^2)}{1-a^2}, \tag{A12}$$

where $K(m) = \int_0^{\pi/2}(1-m\sin^2\theta)^{-1/2}d\theta$ and $E(m) = \int_0^{\pi/2}(1-m\sin^2\theta)^{1/2}d\theta$ are the complete elliptic integrals.

We present also the simple analytical results for important particular case of (i) thin s layer, $d_s \ll \xi_{s,\Delta}$; (ii) weaker s superconductor, $\Delta_s \ll |\Delta_\alpha|$; and (iii) low temperatures, $T \ll T_c^s$. Due to the first condition, the dominating contribution to the gap correction is given by the coordinate independent part $\tilde{\Delta}_{s,0}$, which is determined by the general formula (A12). In the limit of $\Delta_s \ll |\Delta_\alpha|$ we can use the asymptotics of the function $U(a)$ in the limit $a \ll 1$, $U(a) \approx \ln(4/a) - 1$ leading to the following simple result:

$$\frac{\tilde{\Delta}_{s,0}}{\pi T_c} \approx \frac{\xi_s^*}{d_s} \sum_\alpha \frac{\Delta_\alpha-\Delta_s}{\tilde{\gamma}_{B\alpha}|\Delta_\alpha|} \left[\ln\left(\frac{4|\Delta_\alpha|}{\Delta_s}\right) - 1 \right]. \tag{A13}$$

The sign of $\tilde{\Delta}_{s,0}$ determines net effect of the $s_\pm$ superconductor on the s superconductor (positive vs negative proximity). As one can expect, the gaps aligned with Δ_s enhance superconductivity and the gaps antialigned with Δ_s suppress superconductivity in the s superconductor. The relative contributions are mostly determined by the electrical coupling between s superconductor and the $s_\pm$ bands.

Weak spatial dependence of $\tilde{\Delta}_s$ is determined by the components $\tilde{\Delta}_{s,m}$ with $m > 0$. At $T = 0$ these components can be presented as

$$\tilde{\Delta}_{s,m} = -\frac{1}{W_m} \frac{2\xi_{s,\Delta}^2}{d_s\xi_s} \sum_\alpha J_{\alpha,m} \frac{\Delta_s-\Delta_\alpha}{\tilde{\gamma}_{B\alpha}}, \tag{A14}$$

with

$$W_m = \int_0^\infty \frac{dz}{(z^2+1)^{3/2}} \left[1 + \frac{\beta_m^2 z^2}{\sqrt{z^2+\Delta_s^2}+\beta_m^2} \right],$$

$$J_{\alpha,m} = \int_0^\infty dz \frac{z^2}{(z^2+1)\sqrt{z^2+(\Delta_\alpha/\Delta_s)^2}} \frac{1}{\sqrt{z^2+1}+\beta_m},$$

and $\beta_m = (\pi m \xi_{s,\Delta}/d_s)^2$. The first integral can be actually evaluated in the general case,

$$W_m = \frac{1}{\beta_m} \left[\frac{\pi}{2} + \sqrt{\beta_m^2-1} \ln\left(\sqrt{\beta_m^2-1} + \beta_m \right) \right],$$

and it has asymptotics $W_m \approx \ln 2\beta_m$ for $\beta_m \gg 1$. In the limits $|\Delta_\alpha| \gg \Delta_s$ and $\Delta_s\beta_m \gg |\Delta_\alpha|$ the second integral can be evaluated as

$$J_{\alpha,m} \approx \int_0^\infty dz \frac{1}{\sqrt{z^2+(\Delta_\alpha/\Delta_s)^2}} \frac{1}{z+\beta_m} \approx \frac{1}{\beta_m} \ln \frac{2\Delta_s\beta_m}{|\Delta_\alpha|}.$$

Collecting terms, we obtain

$$\tilde{\Delta}_{s,m} \approx -\sum_\alpha \left[1 + \frac{\ln(\Delta_s/|\Delta_\alpha|)}{\ln[2(\pi m\xi_{s,\Delta}/d_s)^2]} \right] \frac{2d_s/\xi_s^*}{(\pi m)^2} \frac{\Delta_s-\Delta_\alpha}{\tilde{\gamma}_{B\alpha}}. \tag{A15}$$

Using relation $(|x|-1)^2 = \frac{1}{3} + 4\sum_{m=1}^\infty \frac{\cos(\pi m x)}{(\pi m)^2}$, we can approximately present the gap correction in real space as

$$\tilde{\Delta}_s(x) \approx \tilde{\Delta}_{s,0} - \frac{d_s}{\xi_s^*} \sum_\alpha \frac{\Delta_s-\Delta_\alpha}{\tilde{\gamma}_{B\alpha}} \left[\frac{(x+d_s)^2}{2d_s^2} - \frac{1}{6} \right] \times \left[1 + \frac{\ln(\Delta_s/|\Delta_\alpha|)}{2\ln(\pi\sqrt{2}\xi_{s,\Delta}/d_s)} \right]. \tag{A16}$$

Correspondingly, for the Green's function for the same limits we derive

$$\tilde{\Phi}_s(\omega,x) \approx \tilde{\Delta}_{s,0} - \pi T_c \frac{\xi_s^*}{d_s} \sum_\alpha \frac{1}{\sqrt{\omega^2+\Delta_\alpha^2}} \frac{\Delta_s-\Delta_\alpha}{\tilde{\gamma}_{B\alpha}} \times \left[1 + \frac{1}{2} \left(\frac{x+d_s}{\xi_{s,\omega}} \right)^2 \right]. \tag{A17}$$

Typically, the spatial dependence of the order parameter is correlated with the sign of proximity: $\tilde{\Delta}_s(x)$ increases towards the boundary for positive proximity and vice versa. Analyzing Eq. (A16), however, we can conclude that this is not always the case. Indeed, the quadratic term changes sign roughly when $(\Delta_1-\Delta_s)/\tilde{\gamma}_{B1}-(\Delta_s+|\Delta_2|)\tilde{\gamma}_{B2}=0$. At this point $\tilde{\Delta}_{s,0}\propto \ln(C\Delta_1/\Delta_s)/\Delta_1-\ln(C|\Delta_2|/\Delta_s)/|\Delta_2|$ and it is negative for $\Delta_1>|\Delta_2|$, meaning that in some narrow range of parameters $\tilde{\Delta}_s(x)$ will increase towards the boundary in spite of negative proximity effect.

2. $s_{\pm}$-wave superconductor

We can evaluate corrections to the $s_{\pm}$ gap parameter and Green's functions following the same general route. The first-order correction to Φ_α with respect to the coupling strength $\gamma_{B\alpha}^{-1}$ is determined by the following equation and boundary conditions:

$$\frac{D_\alpha}{2\omega}G_\alpha\tilde{\Phi}''_\alpha-\tilde{\Phi}_\alpha=-\tilde{\Delta}_\alpha, \tag{A18}$$

$$\xi_\alpha G_\alpha\Phi'_\alpha=\frac{G_s}{\gamma_{B\alpha}}(\Delta_s-\Delta_\alpha),\quad \text{at}\quad x=0, \tag{A19}$$

with $G_\alpha\approx\omega/\sqrt{\omega^2+\Delta_\alpha^2}$ and $\Phi'_\alpha=0$ at $x=-d_\pm$. The self-consistency condition for the linear correction,

$$2\pi T\sum_{\beta,\ \omega>0}\lambda_{\alpha\beta}\frac{G_\beta\tilde{\Phi}_\beta}{\omega}=\tilde{\Delta}_\alpha, \tag{A20}$$

can be rewritten as

$$2\pi T\sum_{\omega>0}\left[\frac{\tilde{\Phi}_\beta}{\sqrt{\omega^2+\Phi_\beta^2}}-\frac{\tilde{\Delta}_\beta}{\omega}\right]+\ln\frac{1}{t}\tilde{\Delta}_\beta =\sum_\alpha\left(\lambda^{-1}_{\beta\alpha}-\lambda^{-1}\delta_{\beta\alpha}\right)\tilde{\Delta}_\alpha, \tag{A21}$$

where λ is the largest eigenvalue of the matrix $\lambda_{\alpha\beta}$.

Similar to the s-wave case, we can split $\tilde{\Phi}_\alpha$ into the contributions induced by the boundary condition and by the correction to the gap parameter, $\tilde{\Phi}_\alpha=\tilde{\Phi}_{\alpha,b}+\tilde{\Phi}_{\alpha,\Delta}$. The equation and the boundary condition for $\tilde{\Phi}_{\alpha,b}$ are

$$\xi^2_{\alpha,\omega}\tilde{\Phi}''_{\alpha,b}-\tilde{\Phi}_{\alpha,b}=0, \tag{A22}$$

$$\xi_\alpha G_\alpha\tilde{\Phi}'_{\alpha,b}=-\frac{G_s}{\gamma_{B\alpha}}(\Delta_s-\Delta_\alpha), \tag{A23}$$

with $\xi^2_{\alpha,\omega}\equiv D_\alpha/(2\sqrt{\omega^2+\Delta_\alpha^2})=\xi^2_{\alpha,\Delta}|\Delta_\alpha|/\sqrt{\omega^2+\Delta_\alpha^2}$ and $\xi^2_{\alpha,\Delta}\equiv D_\alpha/(2|\Delta_\alpha|)$. The solution for $\tilde{\Phi}_{\alpha,b}(x)$ is given by

$$\tilde{\Phi}_{\alpha,b}(x)=\frac{\xi_{\alpha,\omega}}{\xi_\alpha}\frac{G_s}{\gamma_{B\alpha}G_\alpha}(\Delta_s-\Delta_\alpha)\frac{\cosh[(x-d_\pm)/\xi_{\alpha,\omega}]}{\sinh(d_\pm/\xi_{s,\omega})}. \tag{A24}$$

The component $\tilde{\Phi}_{\alpha,\Delta}$ has to be found from the following equations:

$$\xi^2_{\alpha,\omega}\tilde{\Phi}''_{\alpha,\Delta}-\tilde{\Phi}_{\alpha,\Delta}=-\tilde{\Delta}_\alpha, \tag{A25}$$

$$\xi_\alpha G_\alpha\Phi'_{\alpha,\Delta}=0. \tag{A26}$$

We can again find $\tilde{\Phi}_{\alpha,\Delta}(x)$ and $\tilde{\Delta}_\alpha(x)$ using Fourier transform

$$\tilde{\Phi}_{\alpha,\Delta}=\sum_m\tilde{\Phi}_{\alpha,\Delta,m}\cos q_m x,\quad \tilde{\Delta}_\alpha=\sum_m\tilde{\Delta}_{\alpha,m}\cos q_m x,$$

with $q_m=m\pi/d_\pm$. From Eq. (A25) we immediately find

$$\tilde{\Phi}_{\alpha,\Delta,m}=\frac{\tilde{\Delta}_{\alpha,m}}{1+\xi^2_{\alpha,\omega}q_m^2}. \tag{A27}$$

Substituting $\tilde{\Phi}_{\alpha,\Delta}$ into the gap equation, we obtain relation connecting $\tilde{\Delta}_{\alpha,m}$ with $\tilde{\Phi}_{\beta,b,m}$, Fourier components of $\tilde{\Phi}_{\beta,b}(x)$,

$$\begin{aligned}
\tilde{\Delta}_{\alpha,m}&=2\pi T\sum_{\beta,\omega>0}U_{m,\alpha\beta}\frac{\omega^2\tilde{\Phi}_{\beta,b,m}}{\left(\omega^2+\Delta_\beta^2\right)^{3/2}},\\
U_{m,\alpha\beta}&=\left[\lambda^{-1}_{\alpha\beta}-(\lambda^{-1}+\Sigma_{m,\alpha})\delta_{\alpha\beta}\right]^{-1},\\
\Sigma_{m,\alpha}&=2\pi T\sum_{\omega>0}\left[\frac{\omega^2}{\left(\omega^2+\Delta_\alpha^2\right)^{3/2}}\frac{1}{1+\xi^2_{\alpha,\omega}q_m^2}-\frac{1}{\omega}\right]+\ln\frac{1}{t}.
\end{aligned} \tag{A28}$$

Fourier transformation of the result in Eq. (A24) gives

$$\tilde{\Phi}_{s,b,m}=\frac{(2-\delta_m)\,\xi^2_{\alpha,\omega}/\left(d_\pm\xi_\alpha\right)}{1+\xi^2_{\alpha,\omega}q_m^2}\frac{\sqrt{\omega^2+\Delta_\alpha^2}}{\sqrt{\omega^2+\Delta_s^2}}\frac{\Delta_s-\Delta_\alpha}{\gamma_{B\alpha}}. \tag{A29}$$

It is convenient to introduce the degenerate matrix, $w_{\alpha\beta}=\lambda^{-1}_{\alpha\beta}-\lambda^{-1}\delta_{\alpha\beta}$, $w_{11}w_{22}-w_{12}w_{21}=0$. Explicitly, the elements of this matrix are given by

$$\begin{aligned}
w_{11}&=\frac{\sqrt{\lambda_-^2/4+\lambda_{12}\lambda_{21}}-\lambda_-/2}{\det\lambda},\quad w_{12}=-\frac{\lambda_{12}}{\det\lambda},\\
w_{22}&=\frac{\sqrt{\lambda_-^2/4+\lambda_{12}\lambda_{21}}+\lambda_-/2}{\det\lambda},
\end{aligned}$$

with $\lambda_-\equiv\lambda_{11}-\lambda_{22}$ and $\det\lambda\equiv\lambda_{11}\lambda_{22}-\lambda_{12}\lambda_{21}$. The matrix $U_{m,\alpha\beta}=[w_{\alpha\beta}-\Sigma_{m,\alpha}\delta_{\alpha\beta}]^{-1}$ can be presented as

$$\begin{aligned}
\hat{U}_m&=\frac{1}{D_U}\begin{bmatrix}w_{22}-\Sigma_{m,2} & -w_{12}\\ -w_{21} & w_{11}-\Sigma_{m,1}\end{bmatrix},\\
D_U&=-\Sigma_{m,2}w_{11}-\Sigma_{m,1}w_{22}+\Sigma_{m,1}\Sigma_{m,2}.
\end{aligned} \tag{A30}$$

Equations (A27)–(A29) provide full formal solution of the problem.

For convenient comparison with numerical calculations, we present the above results in the reduced form:

$$\begin{aligned}
\tilde{\Phi}_{\alpha,b,m}&=\frac{(2-\delta_m)\,(\xi_\alpha/d_\pm)\sqrt{\omega^2+\Delta_\alpha^2}}{\left[\sqrt{\omega^2+\Delta_\alpha^2}+\left(\frac{m\pi\xi_\alpha}{d_\pm}\right)^2\right]\sqrt{\omega^2+\Delta_s^2}}\frac{\Delta_s-\Delta_\alpha}{\gamma_{B\alpha}},\\
\tilde{\Phi}_{\alpha,\Delta,m}&=\frac{\sqrt{\omega^2+\Delta_\alpha^2}}{\sqrt{\omega^2+\Delta_\alpha^2}+(m\pi\xi_\alpha/d_\pm)^2}\tilde{\Delta}_{\alpha,m},\\
\tilde{\Delta}_{\alpha,m}&=2t\sum_{\beta,\omega>0}U_{m,\alpha\beta}\frac{\omega^2}{\left(\omega^2+\Delta_\beta^2\right)\sqrt{\omega^2+\Delta_s^2}}\\
&\quad\times\frac{2\xi_\beta/d_\pm}{\sqrt{\omega^2+\Delta_\beta^2}+(m\pi\xi_\beta/d_\pm)^2}\frac{\Delta_s-\Delta_\beta}{\gamma_{B\beta}}.
\end{aligned}$$

APPENDIX B: BOUNDARY CONDITIONS IN θ PARAMETRIZATION

In this Appendix we derive the boundary conditions (BCs) in θ parametrization, appropriate for the different SC states we consider. We start with the multiband generalization of the Kupriyanov-Lukichev BCs:

$$\xi_s^* G_s^2 \Phi_s' = \sum_\alpha \frac{\xi_\alpha}{\gamma_\alpha} G_\alpha^2 \Phi_\alpha', \tag{B1a}$$

$$\xi_\alpha G_\alpha \Phi_\alpha' = -\frac{1}{\gamma_{B\alpha}} G_s(\Phi_s - \Phi_\alpha). \tag{B1b}$$

In the aligned case all Φ's can be chosen real. Thus, we have

$$\Phi_\alpha = \omega \tan\theta_\alpha, \quad \Phi_s = \omega \tan\ \theta_s, \quad G_\alpha = \cos\theta_\alpha, \quad G_s = \cos\theta_s,$$

where θ's are also real. With those the BC at the interface for the aligned state simplify to

$$\xi_s^* \theta_s' = \sum_\alpha \frac{\theta_\alpha'}{\gamma_\alpha}, \tag{B2}$$

$$\xi_\alpha \theta_\alpha' = \frac{1}{\gamma_{B\alpha}} \sin(\theta_\alpha - \theta_s). \tag{B3}$$

This corresponds to equations in the reduced units presented in the text.

For the TRSB state the functions $\Phi_{\{s,\alpha\}}$ are complex and we select the following parametrization $\Phi_s = \omega \tan\theta_s e^{i\varphi_s}$ and $\Phi_\alpha = i\omega \tan\theta_\alpha e^{i\varphi_\alpha}$. Taking derivatives

$$\Phi_s' = \omega \left(\frac{\theta_s'}{\cos^2\theta_s} + i\varphi_s' \tan\theta_s \right) e^{i\varphi_s},$$

$$\Phi_\alpha' = i\omega \left(\frac{\theta_\alpha'}{\cos^2\theta_\alpha} + i\varphi_\alpha' \tan\theta_\alpha \right) e^{i\varphi_\alpha},$$

substituting them in Eqs. (B1) and separating real and imaginary parts, we obtain the boundary conditions for the general complex case,

$$\xi_\alpha \theta_\alpha' = -\frac{1}{\gamma_{B\alpha}} [\cos\theta_\alpha \sin\theta_s \sin(\varphi_s - \varphi_\alpha) - \cos\theta_s \sin\theta_\alpha], \tag{B4a}$$

$$\xi_\alpha \varphi_\alpha' \sin\theta_\alpha = \frac{1}{\gamma_{B\alpha}} \sin\theta_s \cos(\varphi_s - \varphi_\alpha), \tag{B4b}$$

$$\xi_s^* \theta_s' = -\sum_\alpha \frac{1}{\tilde{\gamma}_{B\alpha}} [\cos\theta_\alpha \sin\theta_s + \cos\theta_s \sin\theta_\alpha \sin(\varphi_\alpha - \varphi_s)], \tag{B4c}$$

$$\xi_s^* \varphi_s' \sin\theta_s = \sum_\alpha \frac{1}{\tilde{\gamma}_{B\alpha}} \sin\theta_\alpha \cos(\varphi_\alpha - \varphi_s). \tag{B4d}$$

[1] Y. Kamihara, T. Watanabe, M. Hirano, and H. Hosono, J. Am. Chem. Soc. **130**, 3296 (2008).

[2] P. C. W. Chu *et al.*, Physica C **469**, 313 (2009).

[3] J-P. Paglione and R. L. Green, Nat. Phys. **6**, 645 (2010).

[4] P. J. Hirschfeld, M. M. Korshunov, and I. I. Mazin, Rep. Prog. Phys. **74**, 124508 (2011); A. V. Chubukov, Annu. Rev. Cond. Mat. Phys. **3**, 57 (2012).

[5] I. I. Mazin, D. J. Singh, M. D. Johannes, and M. H. Du, Phys. Rev. Lett. **101**, 057003 (2008).

[6] K. Kuroki, S. Onari, R. Arita, H. Usui, Y. Tanaka, H. Kontani, and H. Aoki, Phys. Rev. Lett. **101**, 087004 (2008).

[7] S. Graser, T. A. Maier, P. J. Hirschfeld, and D. J. Scalapino, New J. Phys. **11**, 025016 (2009).

[8] R. Thomale, C. Platt, J. Hu, C. Honerkamp, and B. A. Bernevig, Phys. Rev. B **80**, 180505(R) (2009).

[9] Fa Wang, H. Zhai, Y. Ran, A. Vishwanath, and Dung-Hai Lee, Phys. Rev. Lett. **102**, 047005 (2009).

[10] R. Sknepnek, G. Samolyuk, Y.-B. Lee, and J. Schmalian, Phys. Rev. B **79**, 054511 (2009).

[11] A. V. Chubukov, D. V. Efremov, and I. Eremin, Phys. Rev. B **78**, 134512 (2008).

[12] V. Cvetković and Z. Tešanović, Phys. Rev. B **80**, 024512 (2009).

[13] S. Maiti and A. V. Chubukov, Phys. Rev. B **82**, 214515 (2010).

[14] K. Seo, B. A. Bernevig, and J. Hu, Phys. Rev. Lett. **101**, 206404 (2008).

[15] L. Wray, D. Qian, D. Hsieh, Y. Xia, L. Li, J. G. Checkelsky, A. Pasupathy, K. K. Gomes, C. V. Parker, A. V. Fedorov, G. F. Chen, J. L. Luo, A. Yazdani, N. P. Ong, N. L. Wang, and M. Z. Hasan, Phys. Rev. B **78**, 184508 (2008); K. Nakayama, T. Sato, P. Richard, Y.-M. Xu, Y. Sekiba, S. Souma, G. F. Chen, J. L. Luo, N. L. Wang, H. Ding, and T. Takahashi, Europhys. Lett. **85**, 67002 (2009); K. Terashima *et al.*, Proc. Natl. Acad. Sci. USA **106**, 7330 (2009); Y. Zhang, L. X. Yang, F. Chen, B. Zhou, X. F. Wang, X. H. Chen, M. Arita, K. Shimada, H. Namatame, M. Taniguchi, J. P. Hu, B. P. Xie, and D. L. Feng, Phys. Rev. Lett. **105**, 117003 (2010).

[16] C. C. Tsuei, J. R. Kirtley, C. C. Chi, Lock See Yu-Jahnes, A. Gupta, T. Shaw, J. Z. Sun, and M. B. Ketchen, Phys. Rev. Lett. **73**, 593 (1994); D. J. van Harlingen, Rev. Mod. Phys. **67**, 515 (1995); J. R. Kirtley, C. C. Tsuei, A. Ariando, C. J. M. Verwijs, S. Harkema, and H. Hilgenkamp, Nat. Phys. **2**, 190 (2006).

[17] J. Wu and P. Phillips, Phys. Rev. B **79**, 092502 (2009).

[18] D. Parker and I. I. Mazin, Phys. Rev. Lett. **102**, 227007 (2009).

[19] The necessary requirement for such experiment is the existence of two crystal faces from which tunneling is dominated by the electron and hole bands. This requirement is very hard to meet.

[20] A. D. Christianson, E. A. Goremychkin, R. Osborn, S. Rosenkranz, M. D. Lumsden, C. D. Malliakas, l. S. Todorov, H. Claus, D. Y. Chung, M. G. Kanatzidis, R. I. Bewley, and T. Guidi, Nature **456**, 930 (2008); M. D. Lumsden, and A. D. Christianson, J. Phys.: Condens. Matter **22**, 203203 (2010).

[21] Y. Laplace, J. Bobroff, F. Rullier-Albenque, D. Colson, and A. Forget, Phys. Rev. B **80**, 140501(R) (2009).

[22] R. M. Fernandes, D. K. Pratt, W. Tian, J. Zarestky, A. Kreyssig, S. Nandi, Min Gyu Kim, A. Thaler, Ni Ni, P. C. Canfield, R. J. McQueeney, J. Schmalian, and A. I. Goldman, Phys. Rev. B **81**, 140501(R) (2010).

[23] A. B. Vorontsov, M. G. Vavilov, and A. V. Chubukov, Phys. Rev. B **81**, 174538 (2010); R. M. Fernandes and J. Schmalian, *ibid.* **82**, 014521 (2010).

[24] F. Wei, F. Chen, K. Sasmal, B. Lv, Z. J. Tang, Y. Y. Xue, A. M. Guloy, and C. W. Chu, Phys. Rev. B **81**, 134527 (2010); U. Stockert, M. Abdel-Hafiez, D. V. Evtushinsky, V. B. Zabolotnyy, A. U. B. Wolter, S. Wurmehl, I. Morozov, R. Klingeler, S. V. Borisenko, and B. Büchner, *ibid.* **83**, 224512 (2011); K. Hashimoto, S. Kasahara, R. Katsumata, Y. Mizukami, M. Yamashita, H. Ikeda, T. Terashima, A. Carrington, Y. Matsuda, and T. Shibauchi, Phys. Rev. Lett. **108**, 047003 (2012); H. Kim, M. A. Tanatar, Yoo Jang Song, Yong Seung Kwon, and R. Prozorov, Phys. Rev. B **83**, 100502 (2011); M. A. Tanatar, J.-Ph. Reid, S. René de Cotret, N. Doiron-Leyraud, F. Laliberté, E. Hassinger, J. Chang, H. Kim, K. Cho, Yoo Jang Song, Yong Seung Kwon, R. Prozorov, and Louis Taillefer, *ibid.* **84**, 054507 (2011).

[25] P. Popovich, A. V. Boris, O. V. Dolgov, A. A. Golubov, D. L. Sun, C. T. Lin, R. K. Kremer, and B. Keimer, Phys. Rev. Lett. **105**, 027003 (2010); H. Kim, M. A. Tanatar, Bing Shen, Hai-Hu Wen, and R. Prozorov, arXiv:1105.2265.

[26] J. D. Fletcher, A. Serafin, L. Malone, J. G. Analytis, J. H. Chu, A. S. Erickson, I. R. Fisher, and A. Carrington, Phys. Rev. Lett. **102**, 147001 (2009); C. W. Hicks, T. M. Lippman, M. E. Huber, J. G. Analytis, J. H. Chu, A. S. Erickson, I. R. Fisher, and K. A. Moler, *ibid.* **103**, 127003 (2009); M. Yamashita, N. Nakata, Y. Senshu, S. Tonegawa, K. Ikada, K. Hashimoto, H. Sugawara, T. Shibauchi, and Y. Matsuda, Phys. Rev. B **80**, 220509(R) (2009).

[27] K. Hashimoto, A. Serafin, S. Tonegawa, R. Katsumata, R. Okazaki, T. Saito, H. Fukazawa, Y. Kohori, K. Kihou, C. H. Lee, A. Iyo, H. Eisaki, H. Ikeda, Y. Matsuda, A. Carrington, and T. Shibauchi, Phys. Rev. B **82**, 014526 (2010); J. K. Dong, S. Y. Zhou, T. Y. Guan, H. Zhang, Y. F. Dai, X. Qiu, X. F. Wang, Y. He, X. H. Chen, and S. Y. Li, Phys. Rev. Lett. **104**, 087005 (2010); T. Terashima, M. Kimata, N. Kurita, H. Satsukawa, A. Harada, K. Hazama, M. Imai, A. Sato, K. Kihou, C.-H. Lee, H. Kito, H. Eisaki, A. Iyo, T. Saito, H. Fukazawa, Y. Kohori, H. Harima, and S. Uji, *ibid.* **104**, 259701 (2010); J. K. Dong and S. Y. Zhou, *ibid.* **104**, 259702 (2010).

[28] K. Hashimoto, M. Yamashita, S. Kasahara, Y. Senshu, N. Nakata, S. Tonegawa, K. Ikada, A. Serafin, A. Carrington, T. Terashima, H. Ikeda, T. Shibauchi, and Y. Matsuda, Phys. Rev. B **81**, 220501(R) (2010).

[29] Y. Zhang, Z. R. Ye, Q. Q. Ge, F. Chen, Juan Jiang, M. Xu, B. P. Xie, and D. L. Feng, Nat. Phys. **8**, 371 (2012).

[30] G. Mu, H. Luo, Z. Wang, L. Shan, C. Ren, and H.-H. Wen, Phys. Rev. B **79**, 174501 (2009); G. Mu, B. Zeng, P. Cheng, Z.-S. Wang, L. Fang, B. Shen, L. Shan, C. Ren, and H.-H. Wen, Chinese Phys. Lett. **27**, 037402 (2010); F. Hardy, P. Burger, T. Wolf, R. A. Fisher, P. Schweiss, P. Adelmann, R. Heid, R. Fromknecht, R. Eder, D. Ernst, H. v. Loehneysen, and C. Meingast, Europhys. Lett. **91**, 47008 (2010); K. Gofryk, A. S. Sefat, M. A. McGuire, B. C. Sales, D. Mandrus, J. D. Thompson, E. D. Bauer, and F. Ronning, Phys. Rev. B **81**, 184518 (2010); Dong-Jin Jang, A. B. Vorontsov, I. Vekhter, K. Gofryk, Z. Yang, S. Ju, J. B. Hong, J. H. Han, Y. S. Kwon, F. Ronning, J. D. Thompson, and Tuson Park, New J. Phys. **13**, 023036 (2011); J. Hu, T. M. Liu, B. Qian, A. Rotaru, L. Spinu, and Z. Q. Mao, Phys. Rev. B **83**, 134521 (2011).

[31] C. Martin, H. Kim, R. T. Gordon, N. Ni, V. G. Kogan, S. L. Bud'ko, P. C. Canfield, M. A. Tanatar, and R. Prozorov, Phys. Rev. B **81**, 060505(R) (2010); L. Luan, T. M. Lippman, C. W. Hicks, J. A. Bert, O. M. Auslaender, J. H. Chu, J. G. Analytis, I. R. Fisher, and K. A. Moler, Phys. Rev. Lett. **106**, 067001 (2011); R. Prozorov and V. G. Kogan, Rep. Prog. Phys. **74**, 124505 (2011).

[32] M. A. Tanatar, J.-Ph. Reid, H. Shakeripour, X. G. Luo, N. Doiron-Leyraud, N. Ni, S. L. Bud'ko, P. C. Canfield, R. Prozorov, and Louis Taillefer, Phys. Rev. Lett. **104**, 067002 (2010); J.-Ph. Reid, M. A. Tanatar, X. G. Luo, H. Shakeripour, N. Doiron-Leyraud, N. Ni, S. L. Bud'ko, P. C. Canfield, R. Prozorov, and L. Taillefer, Phys. Rev. B **82**, 064501 (2010); Yo Machida, Kosuke Tomokuni, Takayuki Isono, Koichi Izawa, Yasuyuki Nakajima, and Tsuyoshi Tamegai, J. Phys. Soc. Jpn. **78**, 073705 (2009).

[33] A. B. Vorontsov, M. G. Vavilov, and A. V. Chubukov, Phys. Rev. B **79**, 140507(R) (2009); Y. Bang, Europhys. Lett. **86**, 47001 (2009); A. Glatz and A. E. Koshelev, Phys. Rev. B **82**, 012507 (2010).

[34] J. Guo, S. Jin, G. Wang, S. Wang, K. Zhu, T. Zhou, M. He, and X. Chen, Phys. Rev. B **82**, 180520 (2010).

[35] A. Brinkman, A. A. Golubov, and M. Yu. Kupriyanov, Phys. Rev. B **69**, 214407 (2004).

[36] J. Linder, I. B. Sperstad, and A. Sudbø, Phys. Rev. B **80**, 020503(R) (2009); I. B. Sperstad, J. Linder, and A. Sudbø, *ibid.* **80**, 144507 (2009).

[37] Y. Ota, M. Machida, T. Koyama, and H. Matsumoto, Phys. Rev. Lett. **102**, 237003 (2009); Y. Ota, M. Machida, and T. Koyama, Phys. Rev. B **82**, 140509(R) (2010).

[38] Y. Ota, M. Machida, and T. Koyama, Phys. Rev. B **83**, 060503(R) (2011).

[39] P. Seidel, Supercond. Sci. Technol. **24**, 043001 (2011).

[40] T. K. Ng and N. Nagaosa, Euro. Phys. Lett. **87**, 17003 (2009).

[41] V. Stanev and Z. Tešanović, Phys. Rev. B **81**, 134522 (2010).

[42] E. Berg, N. H. Lindner, and T. Pereg-Barnea, Phys. Rev. Lett. **106**, 147003 (2011).

[43] S. Z. Lin, Phys. Rev. B **86**, 014510 (2012).

[44] For a brief discussion of cases in which superconducting state with broken time-reversal symmetry can appear and an introduction to their properties, see M. Sigrist, Physica B **280**, 154 (2000), and references therein.

[45] A. E. Koshelev, arXiv:1209.5438.

[46] A. M. Bobkov and I. V. Bobkova, Phys. Rev. B **84**, 134527 (2011).

[47] A. E. Koshelev and V. Stanev, Europhys. Lett. **96**, 27014 (2011).

[48] Chr. Bruder, Phys. Rev. B **41**, 4017 (1990).

[49] Y. Ohashi, J. Phys. Soc. Jpn. **65**, 823 (1996).

[50] T. Löfwander, Phys. Rev. B **70**, 094518 (2004).

[51] M. Matsumoto and H. Shiba, J. Phys. Soc. Jpn. **64**, 3384 (1995); **64**, 4867 (1995); S. Kashiwaya and Y. Tanaka, Rep. Prog. Phys. **63**, 1641 (2000).

[52] K. Usadel, Phys. Rev. Lett. **25**, 560 (1970).

[53] A. A. Golubov, E. P. Houwman, J. G. Gijsbertsen, V. M. Krasnov, J. Flokstra, H. Rogalla, and M. Yu. Kupriyanov, Phys. Rev. B **51**, 1073 (1995).

[54] M. Yu. Kupriyanov and V. F. Lukichev, Zh. Eksp. Teor. Phys. **94**, 139 (1988) [Sov. Phys. JETP **67**, 1163 (1988)].

[55] Note that our definitions of $\gamma_{B\alpha}$ is different from the one used in Ref. 53.

[56] H. Shishido, A. F. Bangura, A. I. Coldea, S. Tonegawa, K. Hashimoto, S. Kasahara, P. M. C. Rourke, H. Ikeda, T. Terashima, R. Settai, Y. Onuki, D. Vignolles, C. Proust, B. Vignolle, A. McCollam, Y. Matsuda, T. Shibauchi, and A. Carrington, Phys. Rev. Lett. **104**, 057008 (2010).

[57] F. Rullier-Albenque, D. Colson, A. Forget, P. Thuery, and S. Poissonnet, Phys. Rev. B **81**, 224503 (2010).

[58] J. J. Tu, J. Li, W. Liu, A. Punnoose, Y. Gong, Y. H. Ren, L. J. Li, G. H. Cao, Z. A. Xu, and C. C. Homes, Phys. Rev. B **82**, 174509 (2010).

[59] A. A. Golubov and M. Yu. Kupriyanov, Pis'ma Zh. Eksp. Teor. Fiz. **81**, 419 (2005) [JETP Lett. **81**, 335 (2005)].

[60] W. L. McMillan, Phys. Rev. **175**, 537 (1968).

[61] G. Brammertz, A. Poelaert, A. A. Golubov, P. Verhoeve, A. Peacock, and H. Rogalla, J. Appl. Phys. **90**, 355 (2001).

[62] D. V. Efremov, M. M. Korshunov, O. V. Dolgov, A. A. Golubov, and P. J. Hirschfeld, Phys. Rev. B **84**, 180512(R) (2011).